Asia-Pac. J. Atmos. Sci., 52(2), 107-127, 2016
DOI:10.1007/s13143-016-0013-0
pISSN 1976-7633 / eISSN 1976-7951

Evaluation of Regional Climate Simulations over the CORDEX-EA-II Domain Using the COSMO-CLM Model

Weidan Zhou[1,2], Jianping Tang[1,2,3], Xueyuan Wang[1], Shuyu Wang[1,3], Xiaorui Niu[1,3], and Yuan Wang[1,2]

[1]*School of Atmospheric Sciences, Nanjing University, Nanjing, China*
[2]*Key Laboratory of Mesoscale Severe Weather/Ministry of Education, Nanjing University, Nanjing, China*
[3]*Institute for Climate and Global Change Research, Nanjing University, Nanjing, China*

(Manuscript received 14 October 2015; accepted 25 March 2016)

Abstract: The COSMO-CLM (CCLM) model is applied to perform regional climate simulation over the second phase of CORDEX-East Asia (CORDEX-EA-II) domain in this study. Driven by the ERA-Interim reanalysis data, the model was integrated from 1988 to 2010 with a high resolution of 0.22°. The model's ability to reproduce mean climatology and climatic extremes is evaluated based on various aspects. The CCLM model is capable of capturing the basic features of the East Asia climate, including the seasonal mean patterns, interannual variations, annual cycles and climate extreme indices for both surface air temperature and precipitation. Some biases are evident in certain areas and seasons. Warm and wet biases appear in the arid and semi-arid areas over the northwestern and northern parts of the domain. The simulated climate over the Tibetan Plateau is colder and wetter than the observations, while South China, East China, and India are drier. The model biases may be caused by the simulated anticyclonic and cyclonic biases in low-level circulations, the simulated water vapor content biases, and the inadequate physical parameterizations in the CCLM model. A parallel 0.44° simulation is conducted and the comparison results show some added value introduced by the higher resolution 0.22° simulation. As a result, the CCLM model could be an adequate member for the next stage of the CORDEX-EA project, while further studies should be encouraged.

Key words: Regional climate modeling, Model evaluation, CORDEX-East Asia, COSMO-CLM, ERA-Interim

1. Introduction

Boarded by the Tibetan Plateau and the vast Pacific Ocean, the East Asian climate is characterized by a monsoon system with high climate variability on different spatial-temporal scales (Fu and Zheng, 1998). It has also experienced inter-decadal-scale weakening of summer and winter monsoon circulations since the 1970s (IPCC, 2013). As in many parts of the world, the impacts of climate extremes have been remarkable in East Asia. The simulation of the East Asia climate is a challenge due to the complexity and diversity of processes to be represented. Compared with general circulation models (GCMs), regional climate models (RCMs) with relatively high resolutions can describe more detailed topographical and land surface characteristics and have been widely used in regional climate studies over East Asia (e.g., Suh and Lee, 2004; Gao et al., 2006; Im et al., 2012a, 2012b; Yun et al., 2012; Lee et al., 2013; Zhao, 2013; Oh et al., 2014). IPCC (2014) identified this area vulnerable to the adverse effects of climate change, advancing the application of RCMs in East Asia is still very important (Fu et al., 2005).

RCMs were originally developed in the late 1980s (Dickinson et al., 1989; Giorgi and Bates, 1989), and since then, they have been recognized as flexible and useful downscaling tools for a wide variety of applications (e.g., Giorgi and Mearns, 1999; Rummukainen, 2010; Hong and Kanamitsu, 2014; Xue et al., 2014; Giorgi and Gutowski, 2015). In recent years, new RCMs with non-hydrodynamic and nudging methods have been applied much more frequently in regional climate studies, such as the Weather Research and Forecast (WRF) model (Bukovsky and Karoly, 2009; Bowden et al., 2012) and the Consortium for Small-scale Modeling model in Climate Mode (COSMO-CLM, hereafter CCLM) (Rockel et al., 2008; Rockel and Geyer, 2008; Dobler and Ahrens, 2010; Smiatek, 2014). The CCLM is a non-hydrostatic regional climate model, and it has been widely used for climate simulation and projection in Europe and Africa. The studies using CCLM in Europe show that the model performance is comparable with other state-of-the-art RCMs and even better when using a higher grid resolution (Jaeger et al., 2008; Haslinger et al., 2013; Montesarchio et al., 2014; Bucchignani et al., 2015a). Meanwhile, the CCLM model is generally able to reproduce the overall features of the African climate, although it has some evident deficiencies (Kothe et al., 2014; Panitz et al., 2014; Dosio et al., 2015). The application of the CCLM model has also been carried out in Asia in recent years. The simulation of the Indian summer monsoon shows that the CCLM results are not more accurate than the driving models (Dobler and Ahrens, 2010). On the other hand, Bucchignani et al. (2014) conducted high-resolution (0.125°) simulations using CCLM over China and declared some improvements in reproducing the precipitation and surface temperature during the validation period.

Corresponding Author: Jianping Tang, School of Atmospheric Sciences, Nanjing University, 163 Xianlin Road, Nanjing 210023, China.
E-mail : jptang@nju.edu.cn

To produce an improved generation of regional climate change projections worldwide and provide a framework for better coordination of regional climate downscaling, the World Climate Research Programme (WCRP) initiated the Coordinated Regional Climate Downscaling Experiment (CORDEX) framework (Giorgi et al., 2009). The CORDEX experiments provided an opportunity to evaluate the relative and absolute performances of various RCMs over predefined regions. As one of the 14 branch domains in the framework of CORDEX, CORDEX-East Asia (CORDEX-EA; http://cordex-ea.climate.go.kr/) covers a large area of East Asia with a horizontal resolution of approximately 50 km. Several RCMs driven by "observed" lateral boundary conditions (reanalysis) or the output of global climate models (such as the CMIP5 data) have been evaluated to assess the "structural bias" of the models under the CORDEX-EA framework (Hong and Chang, 2012; Park et al., 2013; Zou et al., 2014a; Lee et al., 2014; Huang et al., 2015). Overall, the RCMs simulate the seasonal mean and annual cycle of the surface air temperature and precipitation well, with the exception that individual models exhibit significant biases in some sub-regions and seasons. By using the CCLM regional climate model, Wang et al. (2013) performed hindcast and projection simulations using ERA-40 reanalysis and the output of the ECHAM5 global climate model inspired by the CORDEX-EA framework. They found that the CCLM reasonably captures the climate features, but significant biases appear in the northern part of the domain and over steep orographic regions. With the development of the RCMs and the demand for higher resolution, CORDEX is now underway to improve the experimental framework leading to its second phase (CORDEX-II). The second phase of CORDEX-East Asia (CORDEX-EA-II) will use the new domain with 0.22° or 25 km resolution. It will be very important and necessary to systematically evaluate the RCM performance when simulating the mean and extreme climates over the CORDEX-EA-II domain.

The dynamical downscaling using RCMs can be classified into four distinct types (Castro et al., 2005). To assess the RCM's performance, the type two simulation method is always used. In this method, the RCM's initial atmospheric conditions have been forgotten, but the results are still dependent on the lateral boundary conditions from global reanalysis data. To evaluate the performance of the CCLM in simulating spatial and temporal characteristics of surface air temperature and precipitation over the CORDEX-EA-II domain, we performed a 23-year (1988-2010) regional climate simulation using the CCLM model. The model is driven by the European Centre for Medium-Range Weather Forecasts (ECMWF) ERA-Interim reanalysis data (hereafter ERAINT; Dee et al., 2011) and has a high resolution of 0.22°. For the purpose of evaluating possible added values from the higher resolution, a coarser grid simulation at a resolution of 0.44° with the same physical parametrizations is carried out simultaneously. The paper is organized as follows: Section 2 describes the CCLM model, experimental design and the observation data. Section 3 presents the evaluation of the model performance in simulating the mean and extreme climate status of the surface air temperature, precipitation, and large-scale circulations. The summary, discussion and conclusions are presented in Section 4.

2. Model and data

a. Model description and experimental design

The CCLM model is a three-dimensional non-hydrostatic regional climate model, which has an Arakawa-C (Arakawa and Lamb, 1977) type horizontal grid on a rotated geographical coordinate system, and a terrain following height coordinates in the vertical direction. The CCLM used in this paper is version 5.0, the detailed descriptions of dynamics, numerics and physical parametrizations can be found in COSMO documentations and the CCLM website (Doms and Baldauf, 2015; Doms et al., 2011; http://www.clm-community.eu).

Wang et al. (2013) and Huang et al. (2015) adapted the CCLM in East Asia following the CORDEX-EA framework at 50-km resolution. In this study, we run the simulation driven by the ERAINT following the CORDEX-EA-II framework with a higher horizontal resolution 0.22° (~25 km). Table 1 lists the basic model configuration parameters of the 0.22° simulation, its domain area covers approximately 9200 km (zonal) × 6200 km (meridional) as in Fig. 1. The parallel 0.44° run (hereafter CCLM44) covers a slightly larger domain because a wider relaxation zone is required. The model's physical parameterization options largely follow the default recommendations of the new CCLM version. The initial inputs and boundary conditions for the large-scale atmospheric fields and sea surface temperatures (SSTs) are from the ERAINT data, which has a resolution of approximately 0.75° × 0.75°.

Table 1. Basic CCLM model configuration parameters for the 0.22° simulation.

Parameter	Longitude	Latitude
Rotated north pole	−63.70°	61.00°
Rotated grid extension	−43.23° to 43.67°	−22.10° to 32.90°
Horizontal grids	396	251
Horizontal resolution	0.22°	
Numerical integration	Runge-Kutta (Wicker and Skamarock, 2002)	
Time step	150s	
Vertical layers	40	
Soil layers	7	
Land surface scheme	TERRA_ML (Schrodin and Heise, 2001)	
Convection scheme	Tiedtke (1989)	
Microphysics scheme	Seifert and Beheng (2001)	
Radiation scheme	Ritter and Geleyn (1992)	
PBL scheme	TKE level 2.5 (Mironov and Raschendorfer, 2001)	

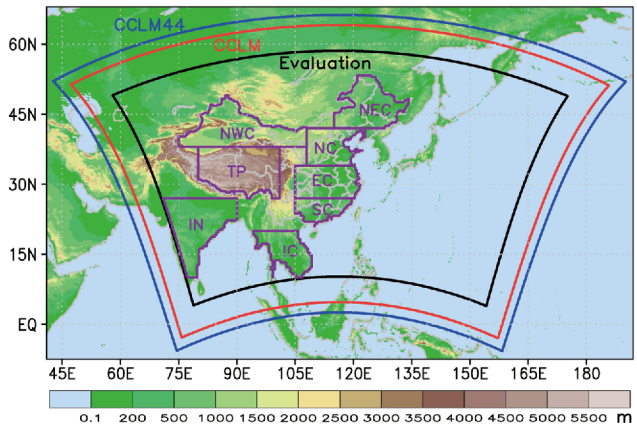

Fig. 1. Model domain and topography. The simulation domain is bounded by the solid red line (CCLM, 0.22° simulation) and blue line (CCLM44, 0.44° simulation), and the evaluation region is outlined with solid black line. There are 8 following sub-regions over land for evaluation purpose: NEC (North East China), NWC (North West China), NC (North China), EC (East China), SC (South China), TP (Tibetan Plateau), IC (Indochina) and IN (India).

The model is integrated continuously for 23 years, starting from 1 January 1988 to 31 December 2010, and the first year (1988) is used as spin-up time.

To better understand the CCLM's capacities on local to region scales, the CORDEX-EA-II domain is divided into eight sub-regions over land (Fig. 1): North East China (NEC), North West China (NWC), North China (NC), East China (EC), South China (SC), Tibetan Plateau (TP), Indochina (IC) and India (IN).

b. Observation datasets

The observation datasets could vary from each other due to different raw data sources, quality control schemes, orographic corrections, and interpolation techniques. To evaluate the performance of the model, we employ a combination of available ground observations, satellite products and reanalysis. The gridded daily and monthly surface observation datasets from the China Meteorological Administration (hereafter CN051; Wu and Gao, 2013) and the monthly surface observation time-series datasets from University of East Anglia Climatic Research Unit (CRU TS v. 3.22, hereafter CRU; Harris et al., 2014) are used for evaluating the surface air temperature and precipitation over land areas. The CN051 dataset covers the mainland China area at a resolution of 0.25° × 0.25°, while the CRU resolution is 0.50° × 0.50° worldwide. For precipitation, the Global Precipitation Climatology Project monthly precipitation data (hereafter GPCP; Huffman et al., 2009) on a 2.5° × 2.5° grid is also used over land and ocean. For the large-scale circulation, the ERA-Interim reanalysis data are compared to the model simulations for evaluation.

All model outputs are remapped to the corresponding observation or reanalysis grids through bilinear (for continuous variables such as temperature, wind speed, etc.) or first-order conservative (for precipitation variables) methods (Jones, 1999), when compared to the above datasets.

3. Results

In this section, we critically analyze the ability of CCLM to reproduce the principal characteristics of the East Asia climatology. We first evaluate the geographical and temporal distribution of the surface air temperature and precipitation. Subsequently, the climate extreme indices derived from the CCLM daily simulation data are presented. Finally, the ability of CCLM to simulate the large-scale circulation and monsoon features over East Asia is exhibited. The results are mainly shown for the 0.22° run (CCLM), unless indicated otherwise (CCLM versus CCLM44).

a. Climatology and variability of surface temperature and precipitation

(1) Seasonal mean climatology

The general ability of the CCLM model to reproduce the seasonal surface climatology is first assessed by comparing the model simulations with the observations during the period of 1989-2010. Figure 2 illustrates the CCLM simulated seasonal mean surface air temperature (2-m temperature) during the period 1989-2010 and the differences between simulations and observations. The observed surface air temperatures are from monthly CRU and CN051 datasets. In winter, CCLM has large warm biases over most of the high latitude region above 40°N and the Indian Peninsula, and the maximum bias exceeds 5.0°C in Siberia. On the other hand, cold biases occur over the Tibetan Plateau and Indochina Peninsula, and the maximum bias exceeds −5.0°C in the Himalayas region. The temperature biases in most regions range from −3.0 to +3.0°C in spring, which are relatively smaller than those in winter. The warm biases are mainly located in India and the Xinjiang province of China, while cold biases are found in the Tibetan Plateau, Northeast China, and Southwest China. The CCLM model tends to overestimate the surface temperature over most of China in summer, and the largest warm bias (approximately 5.0°C) occurs in the Taklimakan Desert and Dzungarian Basin in Xinjiang. The spatial distribution of the temperature bias in autumn is quite similar to that in summer, with a warm bias over most of land region except for the Tibetan Plateau and Indochina Peninsula. However, the magnitudes of the warm biases in autumn are slightly smaller than those in summer.

Table 2 summarizes the mean biases (BIAS), root mean square errors (RMSE) and spatial correlation coefficients (SCOR) of the 22-year averaged seasonal mean surface air temperature between the observations and the CCLM simulation over the East Asia domain and several sub-regions. The spatial correlation coefficients between observations and simulation are high (above 0.85) over most sub-regions except the Indian Peninsula, where the correlation coefficient is relatively

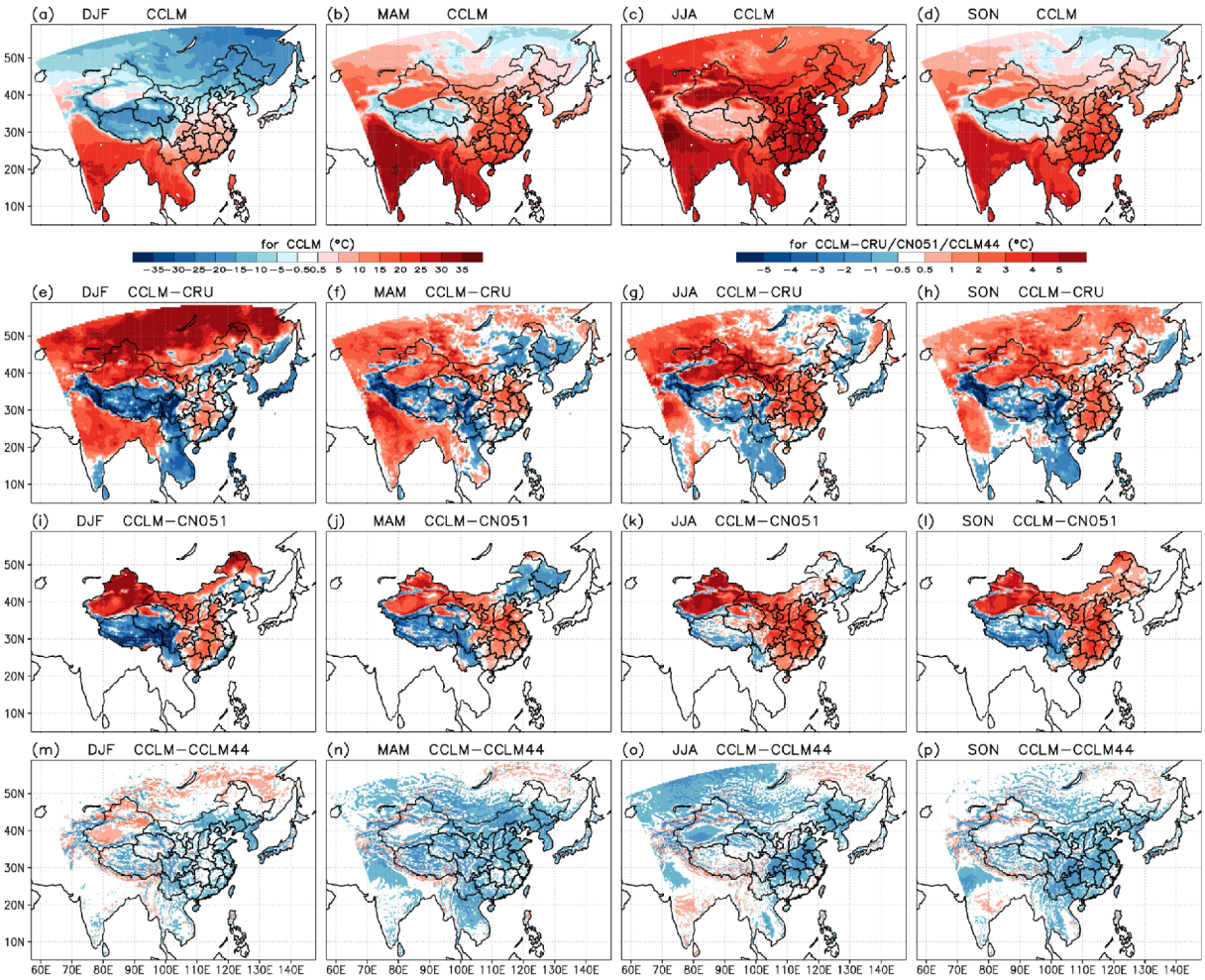

Fig. 2. Observed and simulated seasonal mean 2-m temperatures for the period 1989-2010, for 0.22° CCLM simulations (CCLM, top row), CCLM bias against CRU (CCLM-CRU, second row), CCLM bias against CN051 (CCLM-CN051, third row) and 0.22° CCLM simulations difference against 0.44° CCLM simulations (CCLM-CCLM44, bottom row). The columns from left to right are for winter (DJF), spring (MAM), summer (JJA), and autumn (SON). The units are °C.

lower, especially in autumn. Large temperature RMSEs exist in the Northwest China and Tibetan Plateau regions, especially in winter. The sparse observation stations in these areas may contribute to the large RMSEs. For most sub-regions, the largest RMSEs occur in winter.

The multi-year hindcast bias patterns in this work are similar to previous studies adapting CCLM in this area (e.g., Wang et al., 2013; Bucchignani et al., 2014). Wang et al. (2013) declared that their extreme biases (± 10°C) are only found near the Himalayas and the Karakorum, which might result from an underrepresentation of the steep orography in the CCLM, and the large observation uncertainty in this region could also be another reason for the discrepancies. Bucchignani et al. (2014)'s 0.125° simulation shows qualitatively similar temperature bias maps to Wang et al. (2013) but with slightly lower bias values, suggesting benefits from the higher resolution. Other than qualitative agreement of the bias distributions with the above studies, the comparison of the 0.44° and 0.22° simulations in this study also agree on the small improvements with high-resolution simulation, where the positive/negative signs are opposite between the CCLM-minus-observations and the CCLM-minus-CCLM44 in Fig. 2, especially over the central regions of China and in summer.

Although CRU and CN051 observations largely agree with each other, differences could be found. Taking Fig. 2 for example, in areas with steep terrain and fewer observation stations in western China, the CN051 tends to be a little warmer in these areas than CRU observations, resulting in fewer cold biases along the Himalayas and Tibetan Plateau and more warm biases over Northwest China.

Accurate representation of precipitation and the water cycle is critical for regional climate modeling. Figure 3 presents the CCLM simulated seasonal mean precipitation during 1989-2010 and the differences between simulations and observations. The observed precipitations are from monthly GPCP, CRU, and CN051 datasets. Most of the precipitations over East Asia are strongly influenced by monsoons; in general, high precipitations occur in summer, while low precipitations

Table 2. Multi-year (1989-2010) simulated seasonal mean 2-m temperature (°C) against observations (CRU and CN051): model bias (BIAS), root mean square error (RMSE), and spatial correlation coefficient (SCOR). The sub-regions are M. China (Mainland China), NEC (North East China), NC (North China), EC (East China), SC (South China), NWC (North West China), TP (Tibetan Plateau), IC(Indochina), IN (India), and Land (all land areas).

Region & Obs.	DJF			MAM			JJA			SON		
	BIAS	RMSE	SCOR	BIAS	RMSE	SCOR	BIAS	RMSE	SCOR	BIAS	RMSE	SCOR
M. China												
CRU	0.1	3.2	0.95	−0.2	2.4	0.97	1.0	2.7	0.97	0.4	2.4	0.97
CN051	0.8	3.6	0.94	0.1	2.3	0.98	1.4	2.6	0.98	1.0	2.4	0.97
NEC												
CRU	1.1	2.7	0.92	−0.9	1.4	0.94	−0.1	0.8	0.94	0.7	1.2	0.97
CN051	1.3	2.7	0.93	−1.0	1.3	0.96	0.0	0.7	0.97	1.0	1.3	0.98
NWC												
CRU	3.7	4.4	0.88	1.9	2.8	0.96	3.7	4.4	0.96	2.4	3.0	0.95
CN051	4.7	5.6	0.79	2.1	3.0	0.97	3.6	4.3	0.97	3.0	3.5	0.96
NC												
CRU	−0.2	1.1	0.98	0.5	1.4	0.97	1.6	2.0	0.95	0.9	1.4	0.97
CN051	0.8	1.4	0.97	1.0	1.7	0.98	2.0	2.4	0.94	1.8	2.1	0.98
EC												
CRU	0.2	1.1	0.90	0.8	1.3	0.87	2.1	2.3	0.93	1.2	1.7	0.91
CN051	0.9	1.3	0.91	1.4	1.6	0.92	2.5	2.7	0.94	1.8	2.2	0.92
SC												
CRU	−0.3	1.4	0.89	−0.5	1.0	0.93	0.5	1.0	0.88	0.6	1.3	0.89
CN051	0.6	1.4	0.91	0.4	0.8	0.96	1.2	1.5	0.91	1.4	1.8	0.90
TP												
CRU	−2.6	3.9	0.88	−1.6	2.9	0.93	−0.4	2.3	0.91	−1.3	2.6	0.92
CN051	−2.4	4.0	0.85	−1.7	2.8	0.96	−0.1	1.8	0.96	−1.0	2.3	0.93
IC												
CRU	−2.0	2.6	0.85	0.2	1.1	0.89	−1.2	1.6	0.84	−1.8	2.0	0.90
IN												
CRU	2.2	2.7	0.82	2.1	2.4	0.82	0.2	1.0	0.91	0.4	1.3	0.65
Land												
CRU	1.8	4.2	0.98	0.5	2.2	0.99	0.8	2.3	0.96	0.6	2.1	0.98

occur in winter. During winter, dry biases are found over the coastal areas of Southeast China, the South China Sea and most areas of the Western Pacific Ocean, while wet biases are mainly found over the Tibetan Plateau. The distribution of positive precipitation biases in the northwestern domain and negative precipitation biases over Southeast China in spring is similar to winter, while there are obviously wet biases over Northeast China and low latitudes. In summer, the CCLM tends to underestimate the precipitation over South China, East China, the Korean Peninsula, and the India Peninsula, with the largest underestimation of approximately 3 mm d^{-1} in India and South China. On the other hand, precipitation is over-simulated by 1-3 mm d^{-1} around the Tibetan Plateau. In addition, the precipitation in the low-latitude regions of the Pacific Ocean is significantly overestimated by 3-5 mm d^{-1} compared to the GPCP observation. The model simulates a similar spatial pattern of precipitation biases in autumn over China, vast areas have wet biases except in South China and East China. The model increases the area of the dry biases from South China northeastward to the Pacific Ocean region east of Japan. Additionally, the model underestimates the autumn precipitation by 1-3 mm d^{-1} over the Indochina Peninsula.

Table 3 gives a summary of the 22-year averaged model performance (BIAS, RMSE, and SCOR) for seasonal precipitation between CCLM simulation and the GPCP, CN051 and CRU observations. In general, the CCLM model captures the spatial pattern of the seasonal precipitation over land and sea areas with relatively high correlation. A systematic over-

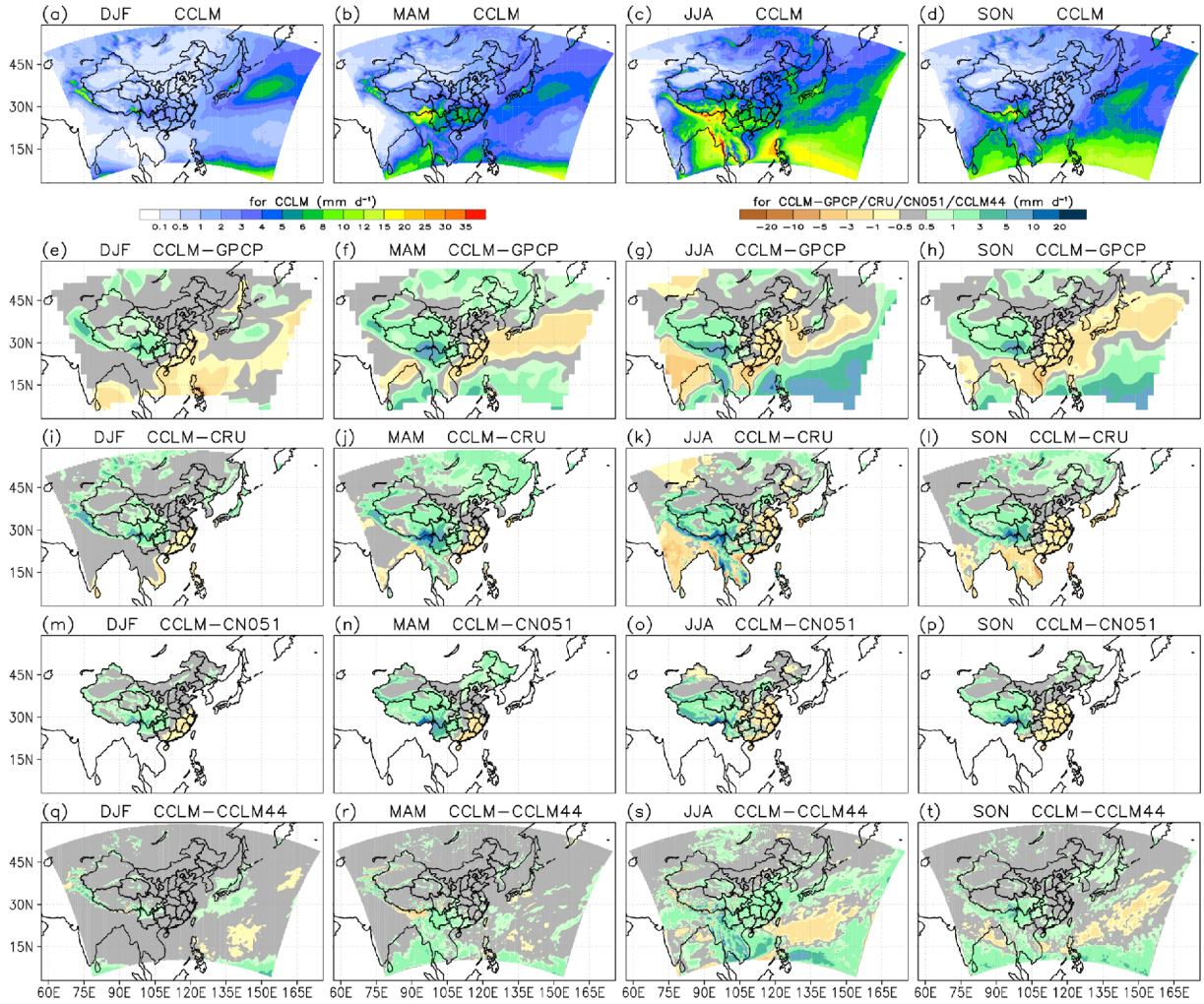

Fig. 3. Observed and simulated seasonal mean precipitation for the period 1989-2010, for 0.22° CCLM simulations (CCLM, top row), CCLM bias against GPCP (CCLM-GPCP, second row), CCLM bias against CRU (CCLM-CRU, third row), CCLM bias against CN051 (CCLM-CN051, fourth row) and 0.22° CCLM simulations difference against 0.44° CCLM simulations (CCLM-CCLM44, bottom row). The columns from left to right are for winter (DJF), spring (MAM), summer (JJA), and autumn (SON). The units are mm d^{-1}.

estimation of 0.3-1.5 mm d^{-1} for the precipitation over land and ocean areas occurs in most seasons except winter. The average precipitation over South China is underestimated in all seasons with relatively low spatial correlation coefficients, and the RMSEs over the Tibetan Plateau and Indochina regions are large.

The simulations of the mean precipitation in our study qualitatively resemble some of the bias features from previous studies adopting the CCLM model over East Asia, although the comparison is not strictly direct due to different forcing data, validation observations, model configurations and simulation periods. The underestimated precipitation around South China and East China and the overestimated precipitation in the northern domain also appeared in the simulations of Wang et al. (2013), Bucchignani et al. (2014) and Huang et al. (2015). The summer and winter precipitation bias patterns over sea areas are also similar to Huang et al. (2015)'s results, while Wang et al. (2013) and Bucchignani et al. (2014) just compared the results over land areas. The differences among our results and the above studies mainly occurred around western Tibet and the Taklamakan desert. Our study, Wang et al. (2013) and Huang et al. (2015) had positive biases compared with the observations, while Bucchignani et al. (2014) reported negative biases. Although some larger positive biases occurred over the southern ocean areas in the 0.22° CCLM simulation and not in the 0.44° experiment, the CCLM run shows smaller negative biases than the CCLM44 run over most areas in the central domain, especially in the rainy summer season, indicating some added values from the higher resolution simulation to the East Asia monsoon region.

In general, the CCLM model can basically reproduce the spatial characteristics of seasonal surface temperature, although significant biases exist in some sub-regions and seasons, especially in winter. The model can also simulate the dis-

Table 3. Multi-year (1989-2010) simulated seasonal mean precipitation (mm d^{-1}) against observations (CRU, CN051 and GPCP): model bias (BIAS), root mean square error (RMSE) and spatial correlation coefficient (SCOR). The sub-regions are M. China (Mainland China), NEC (North East China), NC (North China), EC (East China), SC (South China), NWC (North West China), TP (Tibetan Plateau), IC(Indochina), IN (India), Land (all land areas), Sea (all seas), and All (entire CORDEX-EA-II domain).

Region & Obs.	DJF			MAM			JJA			SON		
	BIAS	RMSE	SCOR	BIAS	RMSE	SCOR	BIAS	RMSE	SCOR	BIAS	RMSE	SCOR
M. China												
CRU	0.5	1.0	0.36	1.1	2.0	0.62	0.8	2.2	0.73	0.6	1.7	0.43
CN051	0.5	1.0	0.39	1.0	2.1	0.63	0.7	2.5	0.62	0.6	1.7	0.40
NEC												
CRU	0.4	0.4	0.51	1.0	1.1	0.79	0.1	0.6	0.74	0.6	0.7	0.76
CN051	0.3	0.4	0.73	1.0	1.1	0.82	0.1	0.4	0.83	0.6	0.6	0.86
NWC												
CRU	0.4	0.6	0.45	0.6	1.0	0.72	0.3	1.3	0.32	0.4	0.7	0.50
CN051	0.4	0.6	0.67	0.5	1.0	0.76	0.2	1.0	0.80	0.3	0.6	0.78
NC												
CRU	0.2	0.2	0.32	0.4	0.5	0.52	0.2	1.0	0.53	0.0	0.4	0.15
CN051	0.2	0.2	0.41	0.4	0.5	0.59	0.1	0.9	0.63	0.0	0.4	0.27
EC												
CRU	0.2	0.8	0.34	0.2	0.9	0.83	–0.6	1.2	0.35	–0.8	0.9	0.60
CN051	0.1	0.9	0.37	0.1	1.0	0.83	–0.9	1.4	0.50	–0.8	1.0	0.61
SC												
CRU	–0.2	0.7	0.33	–0.3	1.4	0.37	–0.2	1.8	0.11	–0.8	1.0	0.31
CN051	–0.4	0.8	0.35	–0.3	1.4	0.43	–0.5	1.5	0.39	–0.9	0.9	0.44
TP												
CRU	0.8	1.5	0.03	1.9	3.1	0.64	2.6	3.6	0.74	1.9	2.8	0.75
CN051	0.9	1.5	0.59	2.0	3.1	0.77	2.7	4.2	0.48	1.9	2.9	0.70
IC												
CRU	–0.6	0.9	0.64	0.5	1.2	0.36	1.2	6.6	0.43	–2.1	2.9	0.72
IN												
CRU	–0.1	0.3	0.52	–0.3	0.6	0.88	–2.0	2.7	0.84	–0.2	1.0	0.79
Land												
CRU	0.4	1.2	0.41	0.8	1.9	0.67	0.3	2.8	0.78	0.3	1.7	0.71
GPCP	0.3	0.9	0.59	0.7	1.6	0.73	0.2	2.0	0.85	0.3	1.3	0.74
Sea												
GPCP	–0.4	1.0	0.85	0.3	1.4	0.67	1.5	3.2	0.72	0.6	2.4	0.69
All												
GPCP	0.0	1.0	0.82	0.5	1.5	0.73	0.8	2.6	0.80	0.4	1.9	0.81

tribution of seasonal precipitation but tends to underestimate the precipitation over South and East China while overestimating them over the Tibetan Plateau region. Although the CN051 dataset contains more station observations than CRU in China, the station density over Tibet and the desert areas is still very low, which may cause higher uncertainties, especially when associated with complex terrains (Wu and Gao, 2013).

(2) Interannual variation

Taylor diagrams (Taylor, 2001) are used to assess the model's ability to simulate the interannual variation of the seasonal surface temperature and precipitation in each subregion. The correlation and variance are calculated from the interannual variation of the regionally-averaged seasonal-mean precipitation for the period 1989-2010. Figure 4 shows the Taylor diagrams of the seasonal-mean surface temperature.

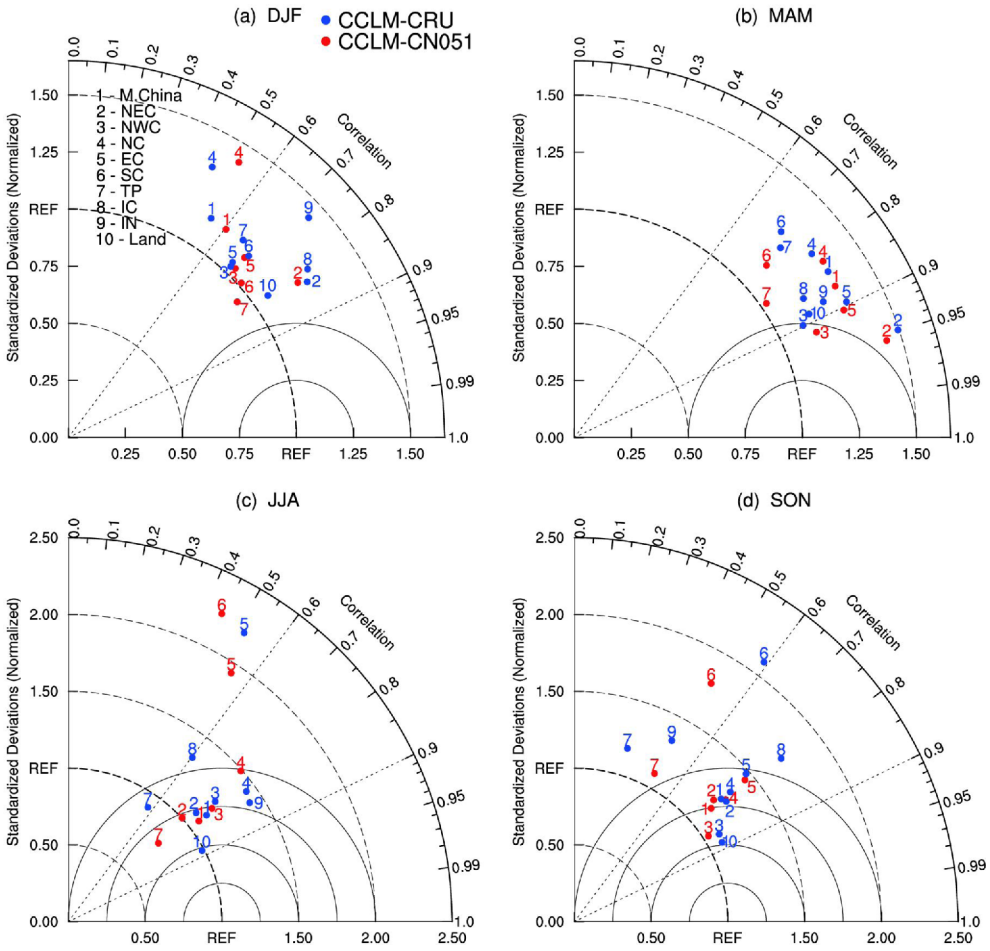

Fig. 4. Taylor diagrams of interannual correlation and variance of simulated area-averaged seasonal-mean 2-m temperature in relation to observation datasets for the sub-regions: M. China (Mainland China), NEC (North East China), NC (North China), EC (East China), SC (South China), NWC (North West China), TP (Tibetan Plateau), IC (Indochina), IN (India), and Land (all land areas). There is one data point out of the plotting area: (c) CCLM-CRU 6-SC (Dev., Cor.) = (2.86, 0.42).

The CCLM largely reproduces the interannual variation of the seasonal-mean temperature over land areas with the correlation coefficients close to 0.9, but the performance differs between seasons and sub-regions. The model simulates the interannual variance higher than the observation over most of the sub-regions in all seasons. The performance of the simulation of the seasonal-mean temperature interannual variation over the South China region is lower than those over other regions in all seasons except for winter. The CCLM outperforms in spring with a higher correlation coefficient compared with other seasons over almost all sub-regions.

Compared to the temperature, the CCLM performs worse in the representation of the interannual variation of the seasonal-mean precipitation (Fig. 5). The temporal correlation of the regionally-averaged seasonal-mean precipitation between the CCLM simulation and the observations is relatively low (below 0.6) over most sub-regions in summer and autumn, particularly in South China and India. The CCLM generally produces much higher interannual variance, especially over regions with complex topographies (e.g., the Tibetan Plateau) and fewer observations (e.g., Northwest China). When evaluating the statistical results for all of the land and ocean areas and the entire East Asia domain, the model shows relatively better performance in the simulation of the interannual variation than those for small analysis sub-regions. The difference between CCLM-CRU and CCLM-CN051 over East Asia is marked in summer, suggesting that gridded precipitation observations could vary a lot more than temperature even in areas with relatively dense observations. Because CN051 adopted similar interpolation techniques to the CRU data (Wu and Gao, 2013), this difference mainly comes from the inclusion of more observation stations in CN051. Thus, a higher observation resolution is essential for regional climate downscaling evaluations, especially for highly localized variables such as precipitation.

(3) Annual cycles

The simulated and observed annual cycles of surface

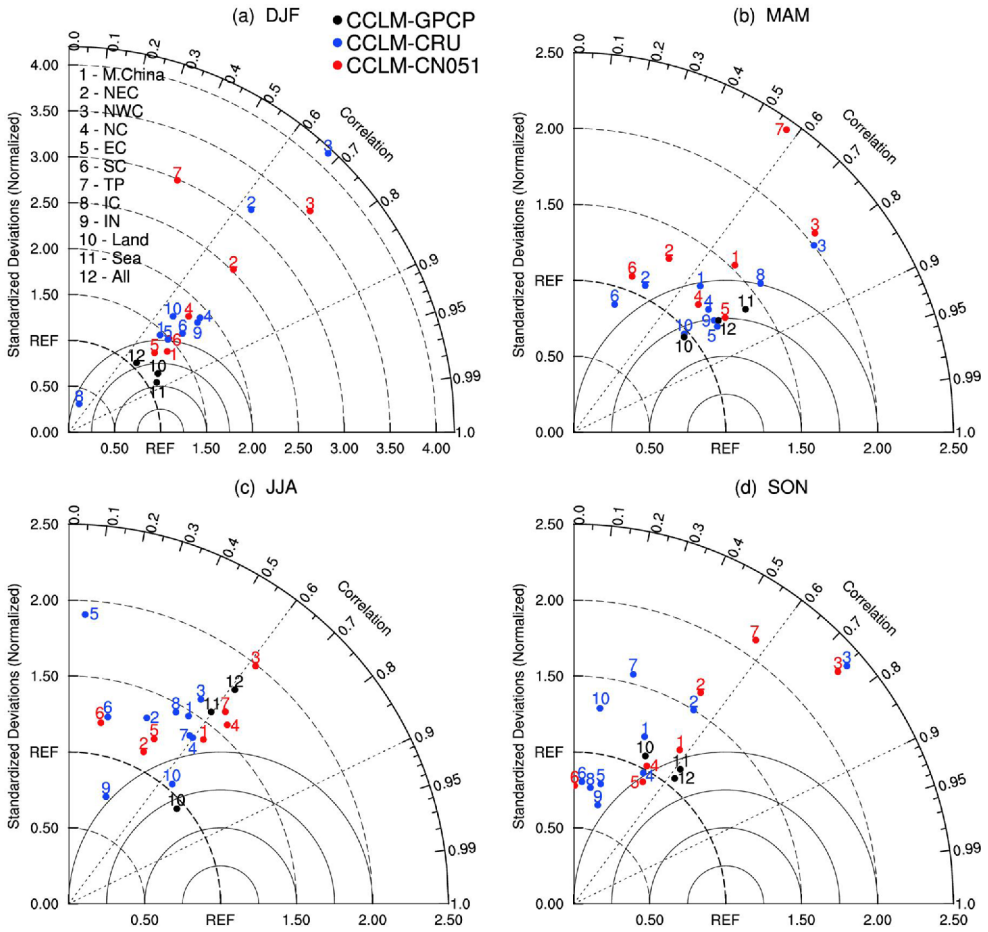

Fig. 5. Taylor diagrams of interannual correlation and variance of simulated area-averaged seasonal-mean precipitation in relation to observation datasets for the sub-regions: M. China (Mainland China), NEC (North East China), NC (North China), EC (East China), SC (South China), NWC (North West China), TP (Tibetan Plateau), IC (Indochina), IN (India), Land (all land areas), Sea (all seas), and All (whole CORDEX-EA-II domain). There are two data points out of the plotting area: (a) CCLM-CRU 7-TP (Dev., Cor.) = (1.36, −0.02); (b) CCLM-CRU 7-TP (Dev., Cor.) = (1.06, −0.03).

temperature over sub-regions in East Asia are demonstrated in Fig. 6. The hottest season for most East Asia regions is summer, while the coldest is winter. However, for the southern parts of the domain, such as the Indochina and India regions, the hot season comes in spring (Indochina) or spring to summer (India). The CCLM describes the annual cycles of surface air temperature over mainland China, Northeast China, South China and the land areas of East Asia (Figs. 6a, b, f, j) with very high correlation coefficients, low BIASs and RMSEs (approximately 1°C). The annual cycles are also captured fairly well over most regions but with some warm biases in summer in North China, summer in East China, and winter and spring in India, as well as cold biases over the Tibetan Plateau and Indochina Peninsula. Compared to other sub-regions, Northwest China has the largest BIAS and RMSE for the temperature of the annual cycle, which reaches approximately 3°C. Figure 7 shows the regionally-averaged seasonal variation in monthly-mean precipitation. Most of the precipitations occur in the summer half of the year for all sub-regions. Overall, the CCLM simulates the seasonal variations of monthly mean precipitation well over land areas in East Asia, with correlation coefficients higher than 0.95 and RMSE less than 0.5 mm d^{-1}. The model generally overestimates the precipitation in warm seasons over ocean areas, with the RMSE up to 1 mm d^{-1}. The performance of CCLM in simulating the annual amplitude of precipitation is clearly dependent on the geographic location and season. Over North China, East China, and South China, the model output satisfactorily follows the course of the year. However, the annual amplitude of precipitation is significantly overestimated in mainland China, the Northwest China sub-region, and in particular, the Tibetan Plateau has BIAS and RMSE that exceed 2 mm d^{-1}. In India, the strongly underestimated summer precipitation leads to a significant underestimation of the annual amplitude of precipitation.

It still should be taken into account that the observational data qualities in low populated areas such as Northwest China and the Tibetan Plateau could be questionable due to low density of original station values and the decrease in the

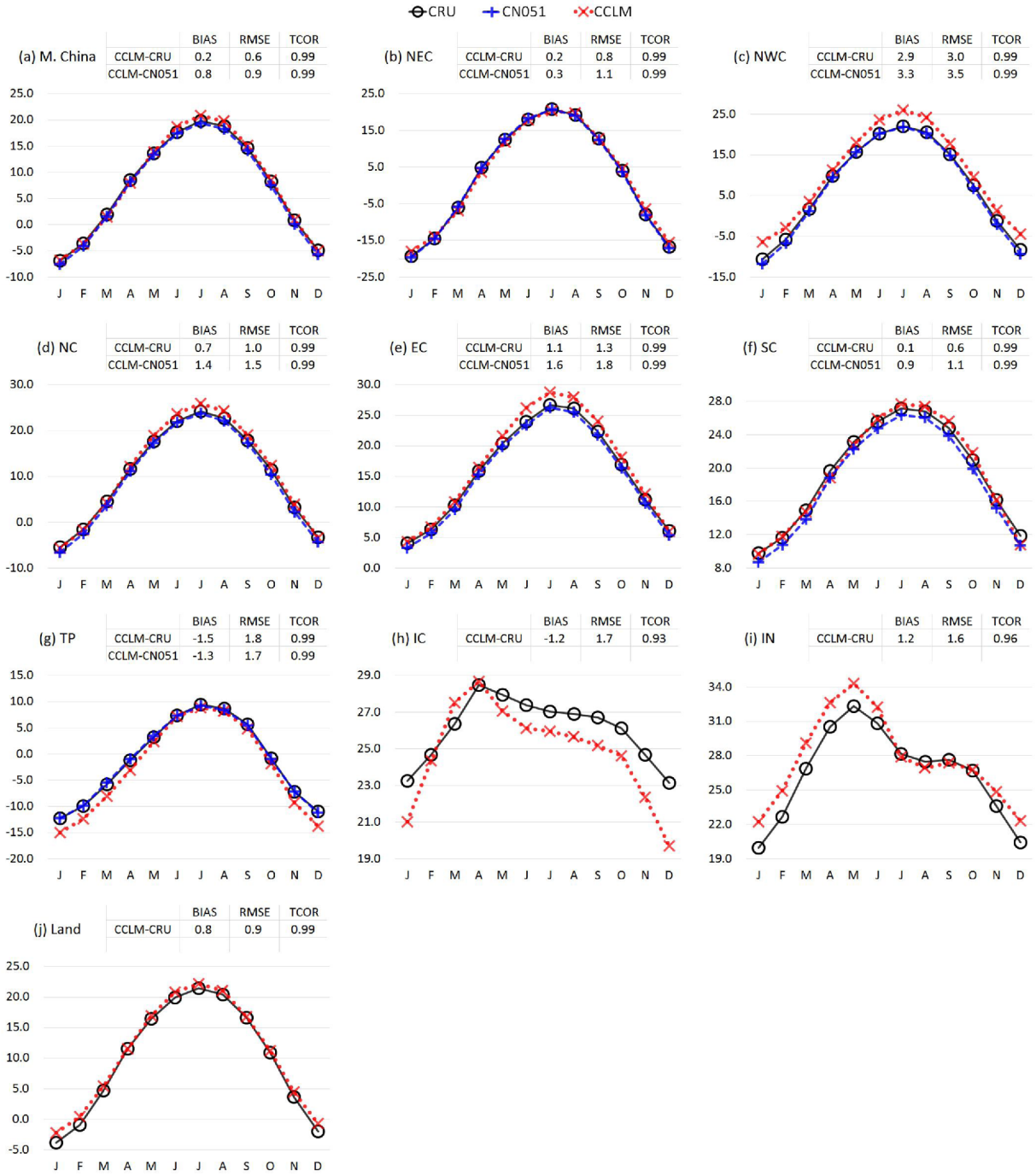

Fig. 6. Annual cycles of observed and simulated 2-m temperatures (°C) for the period 1989-2010, averaged for the sub-regions M. China (Mainland China), NEC (North East China), NWC (North West China), NC (North China), EC (East China), SC (South China), TP (Tibetan Plateau), IC (Indochina), IN (India) and Land (Land areas). The BIAS (model bias), RMSE (root mean square error) and TCOR (correlation coefficient over time) are for the simulation (CCLM) against the observations (CRU and CN051).

accuracy of the gridded observational data interpolation in complex terrains (Sun et al., 2014).

b. Climate extremes

Extreme climate events are identified if, during a specific period, certain climate elements or their statistics are far beyond their normal ranges and exceed specific thresholds (AghaKouchak et al., 2013). Extreme indices, which are designed to directly reflect the frequency and intensity of extreme events, have been widely applied to studies of extreme climate events all over the world (e.g., Frich et al., 2002; Sillmann et al., 2013). In this study, we use the climate extremes indices defined by the Expert Team on Climate

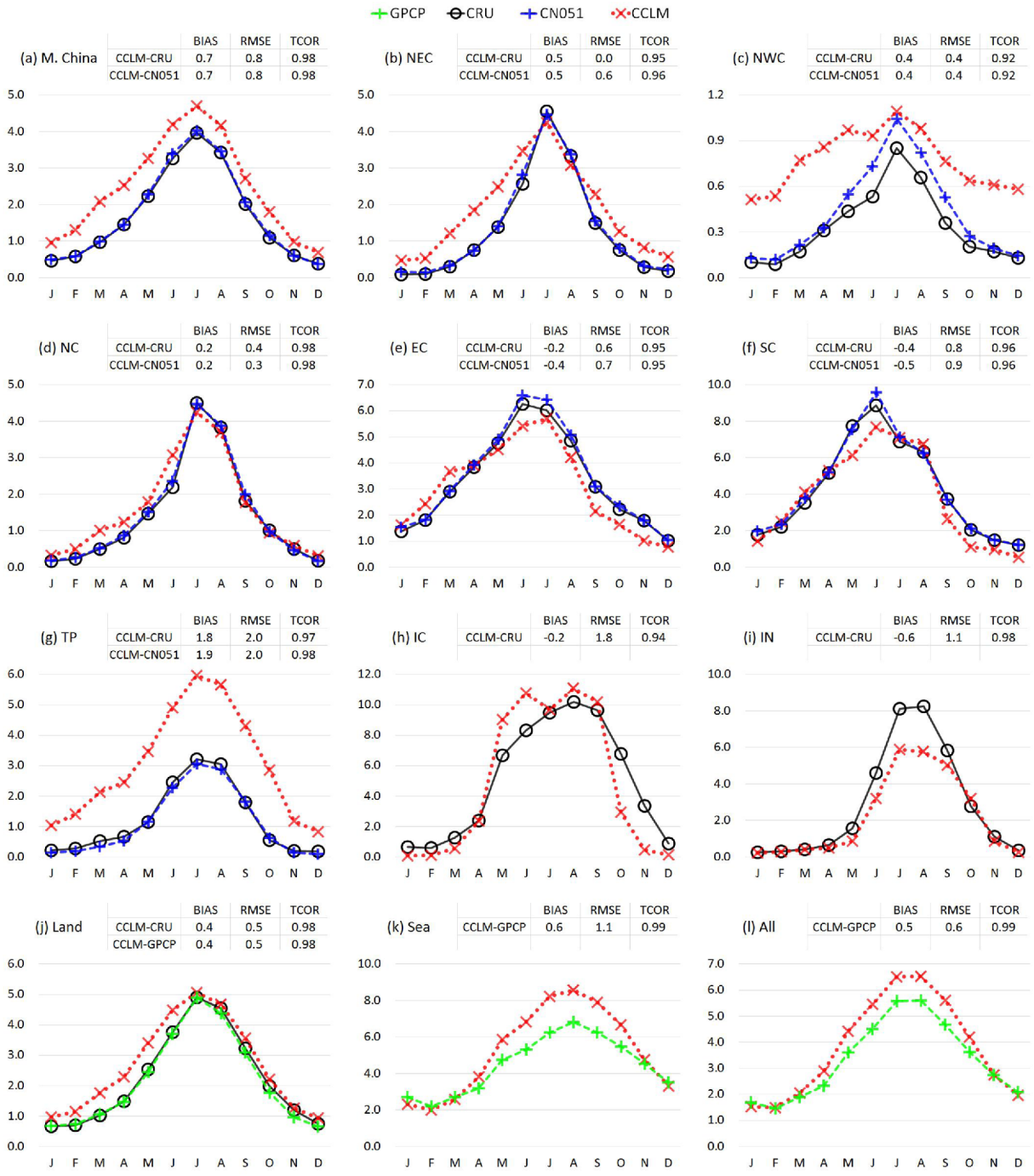

Fig. 7. Annual cycles of observed and simulated precipitation (mm d^{-1}) for the period 1989-2010, averaged for the sub-regions M. China (Mainland China), NEC (North East China), NWC (North West China), NC (North China), EC (East China), SC (South China), TP (Tibetan Plateau), IC (Indochina), IN (India), Land (Land areas), Sea (all seas) and All (entire CORDEX-EA-II domain). The BIAS (model bias), RMSE (root mean square error) and TCOR (correlation coefficient over time) are for the simulation (CCLM) against the observations (CRU, CN051 and GPCP).

Change Detection and Indices (ETCCDI) (Sillmann et al., 2013), which cover the intensity, duration and frequency aspects of extreme temperature and precipitation (Table 4).

To evaluate the capability of CCLM in simulating the climate extremes, the characteristic spatial and temporal distributions of extremes indices calculated from daily CN051 observations and CCLM simulations are compared. Figure 8 shows the spatial distribution of 22-year averaged surface temperature extreme indices from observation and the biases between observation and simulation. The CCLM model generally well

Table 4. The extreme temperature and precipitation indices calculated in this paper following Frich et al. (2002). Precise definitions could be found at http://etccdi.pacificclimate.org/list_27_indices.shtml.

ID	Indicator	Definitions	Units
Temperature - Intensity			
TNn	Min Tmin	Minimum value of daily minimum temperature	°C
TXx	Max Tmax	Maximum value of daily maximum temperature	°C
Temperature - Duration			
GSL	Growing season length	Annual (1 January to 31 December in NH, 1 July to 30 June in SH) count between first span of at least 6 days with TG (daily mean temperature) > 5°C and first span after 1 July (1 January in SH) of 6 days with TG < 5°C	days
Temperature - Frequency			
FD	Frost days	Annual count when daily minimum temperature < 0°C	days
SU	Summer days	Annual count when daily maximum temperature > 25°C	days
Precipitation - Intensity			
Rx5day	Max 5-d precipitation amount	Maximum consecutive 5-d precipitation	mm
R95p	Very wet days	Annual total precipitation from days > 95th percentile	mm
Precipitation - Duration			
CWD	Consecutive wet days	Maximum number of consecutive days when precipitation ≥ 1 mm	days
CDD	Consecutive dry days	Maximum number of consecutive days when precipitation < 1 mm	days
Precipitation - Frequency			
R10mm	Number of heavy precipitation days	Annual count when precipitation ≥ 10 mm	days

reproduces the spatial pattern of the temperature extreme indices. The model overestimates the TNn (minimum daily Tmin) over regions north of 35°N but underestimate it along the coastal area of South China, East China, and Tibetan Plateau. The spatial pattern of TXx (maximum daily Tmax) is similar to that of mean surface temperature, which shows that warm biases exist over most regions of China except for the eastern parts of Northeast China and the Tibetan Plateau. The model simulated bias of GSL (annual count between first span of mean temperature > 5°C and first span after < 5°C) is relatively small ranging from −30 to +30 days. The FD index (annual count when the daily minimum temperature < 0°C) shows the opposite pattern of TNn, indicating that the CCLM performance is similar for extreme low temperature intensities and frequencies. Generally, warm biases occur in northern China and fewer cool biases occur in southern China. The distribution of the bias pattern of the SU index (annual count when daily maximum temperature > 25°C) is different from that of TXx, especially in the Yunnan province of Southwest China and Northeast China, indicating that the frequency of hot events is underestimated there more than the intensity of the extreme hot events.

For the precipitation extreme indices (Fig. 9), the CCLM shows relatively lower performance in simulating the spatial pattern than the above temperature indices. It significantly overproduced the Rx5day (maximum 5-d precipitation amount) over most regions in China, with the maximum overestimation (above 150%) over southern Xinjiang and the Tibetan Plateau. The distribution of the R95p biases (annual total precipitation from days > 95th percentile) is consistent with that of Rx5day but has obvious underestimations greater than −90 mm over South China and East China. The CWD (consecutive wet days) simulated by the CCLM agrees well with the observation, with high values (above 10 days) over southern Tibet and Southwest and South China, and the biases are relatively small, ranging from −30 to +30 days. In contrast, the distribution of CDD (consecutive dry days) from the CCLM simulation shows almost the opposite pattern from the observation. There are large bias areas covering nearly all of China, with positive biases over South China, East China, and several areas in Xinjiang, and negative biases over other regions of China. This bias pattern is quite similar to that of the seasonal precipitation, and the dry (wet) bias contributes to the positive (negative) biases of the CDD. The bias of R10mm (annual count when precipitation ≥ 10 mm) shows positive (wetter) values over the Tibetan Plateau and Southwest China and negative (drier) values over Southeast China. In general, the mean extreme precipitation is overestimated by the CCLM in the western and northern parts of China and underestimated in the eastern and southern parts of China.

Figure 10 shows the interannual variation of the domain-averaged surface temperature and precipitation extreme indices from observation (CN051) and simulation (CCLM) during 1989-2010. The statistical scores (BIAS, RMSE, and TCOR (temporal correlation coefficient)) are also presented. The CCLM simulated interannual variations of the extreme indices agree well with the observations, with the temporal correlations above 0.5 except for the CDD index. However, there are

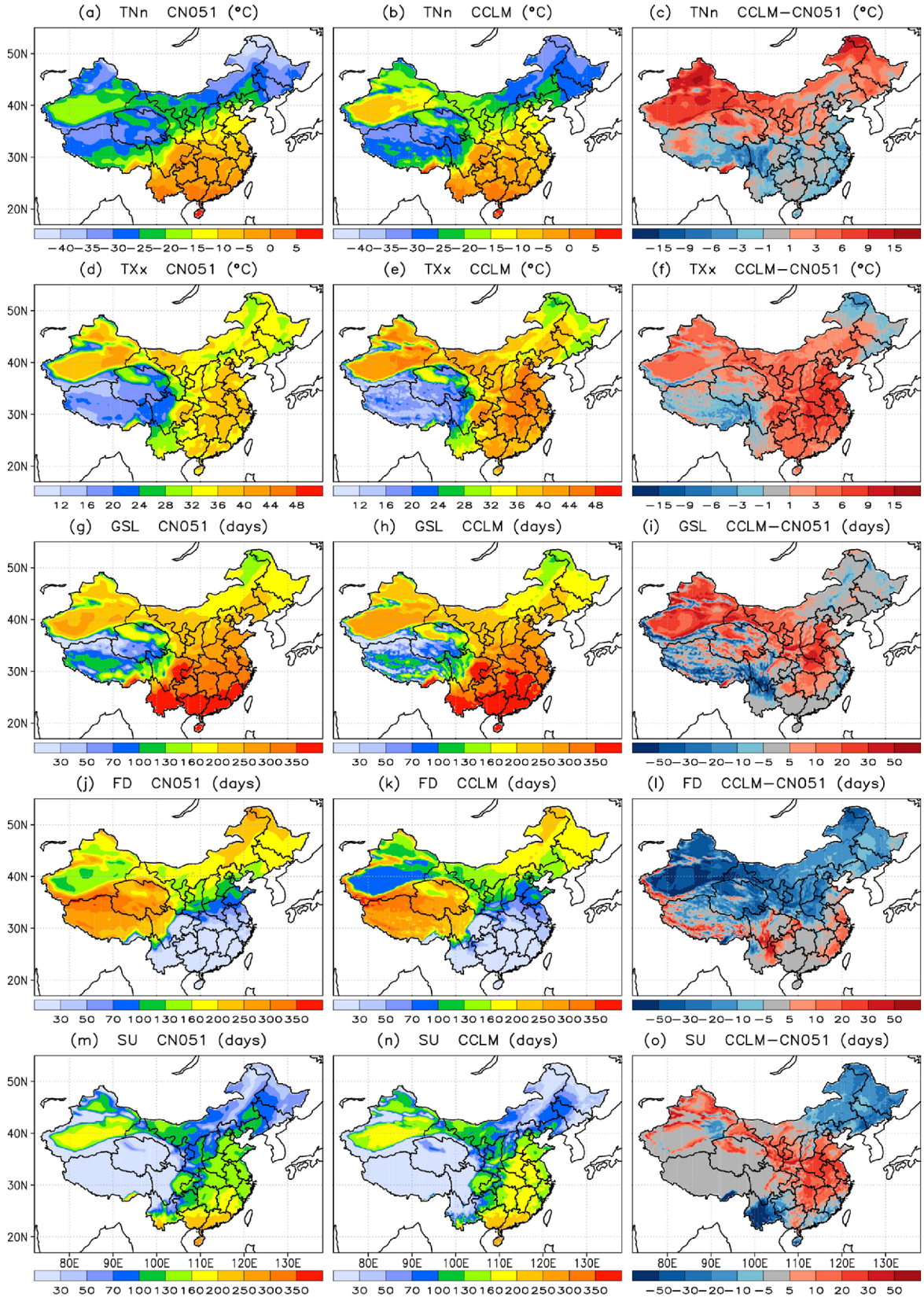

Fig. 8. Climate extreme temperature indices for the period 1989-2010 of observation (CN051), the simulation (CCLM), and the CCLM-CN051 biases: TNn, Txx, GSL, FD, and SU from top to bottom rows. The indices' computation methods are from Frich et al. (2002) and listed in Table 4.

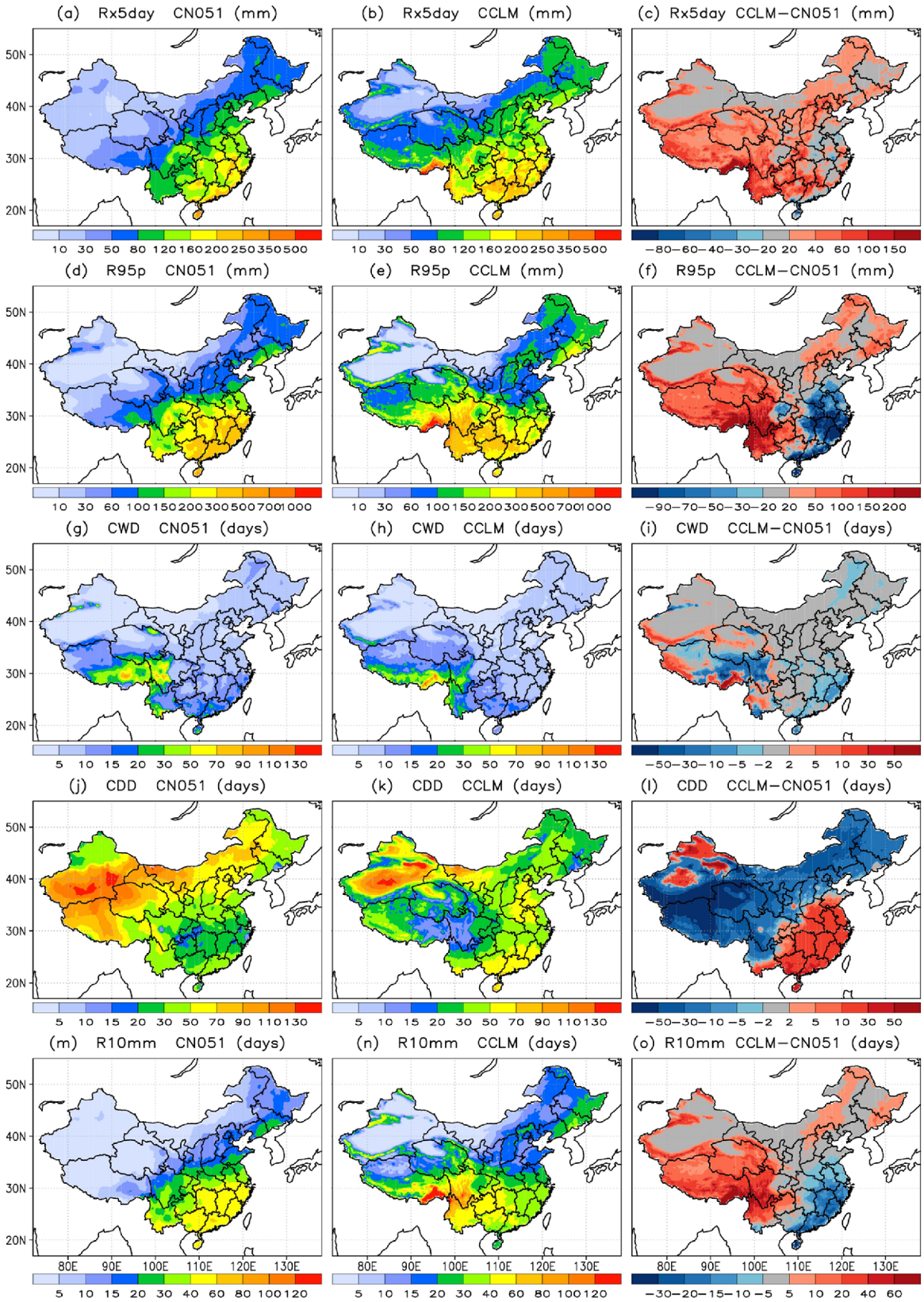

Fig. 9. Climate extreme precipitation indices for the period 1989-2010 from the observation (CN051), simulation (CCLM), and CCLM-CN051 biases: Rx5day, R95p, CWD, CDD, and R10mm from top to bottom rows. The indices' computation methods are from Frich et al. (2002) and listed in Table 4.

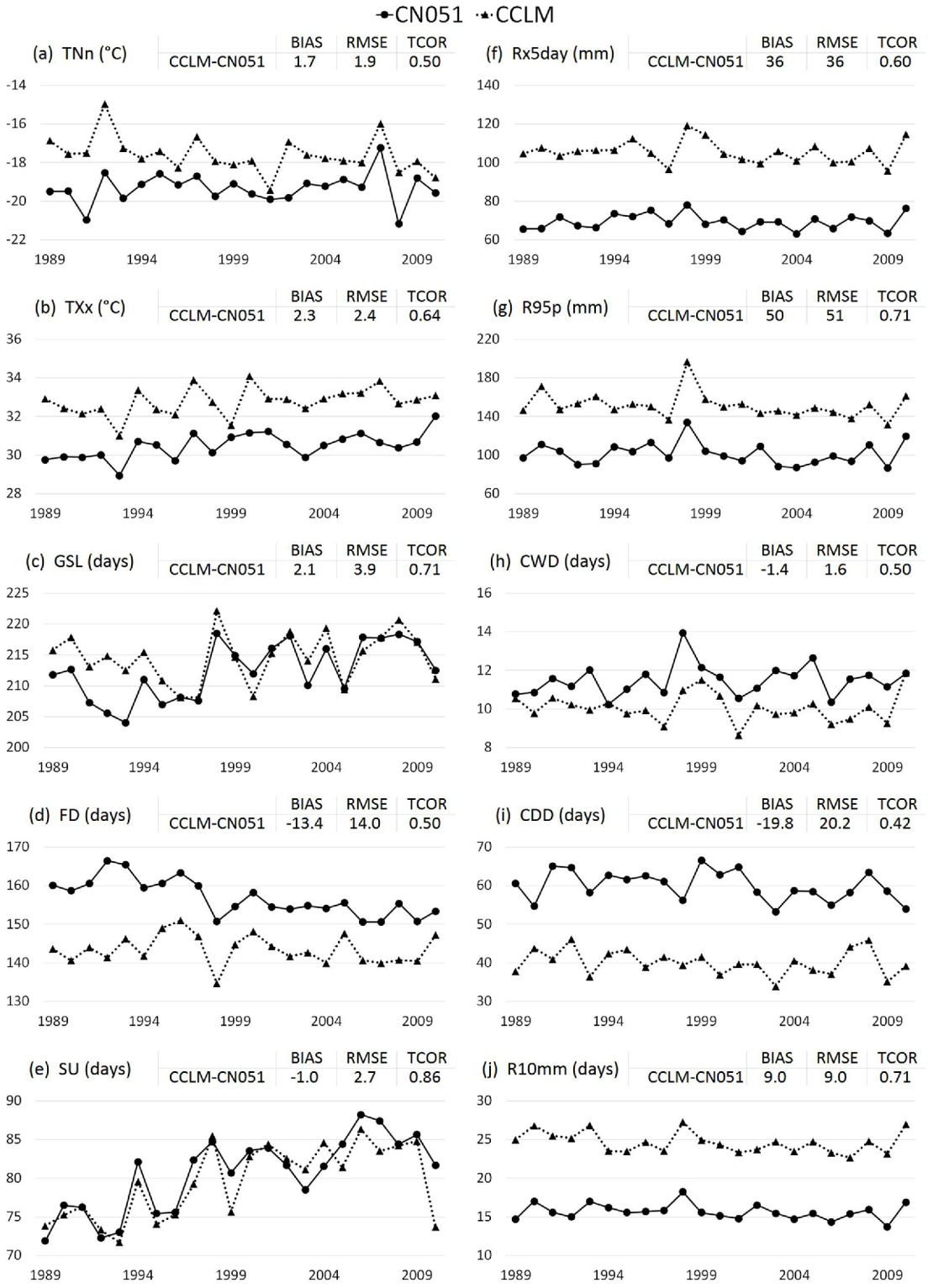

Fig. 10. Domain averaged climate extremes indices for the period 1989-2010. The BIAS (model bias), RMSE (root mean square error) and TCOR (correlation coefficient over time) are for the simulation (CCLM) against the observations (CN051).

obvious biases between observation and simulation for TXx, FD, Rx5day, R95p CDD and R10mm. The magnitudes of the RMSEs are consistent with the BIAS, which means that the CCLM simulations of these climate extreme indices have systematic errors. The differences in the precipitation indices between observation and simulation show significant wet

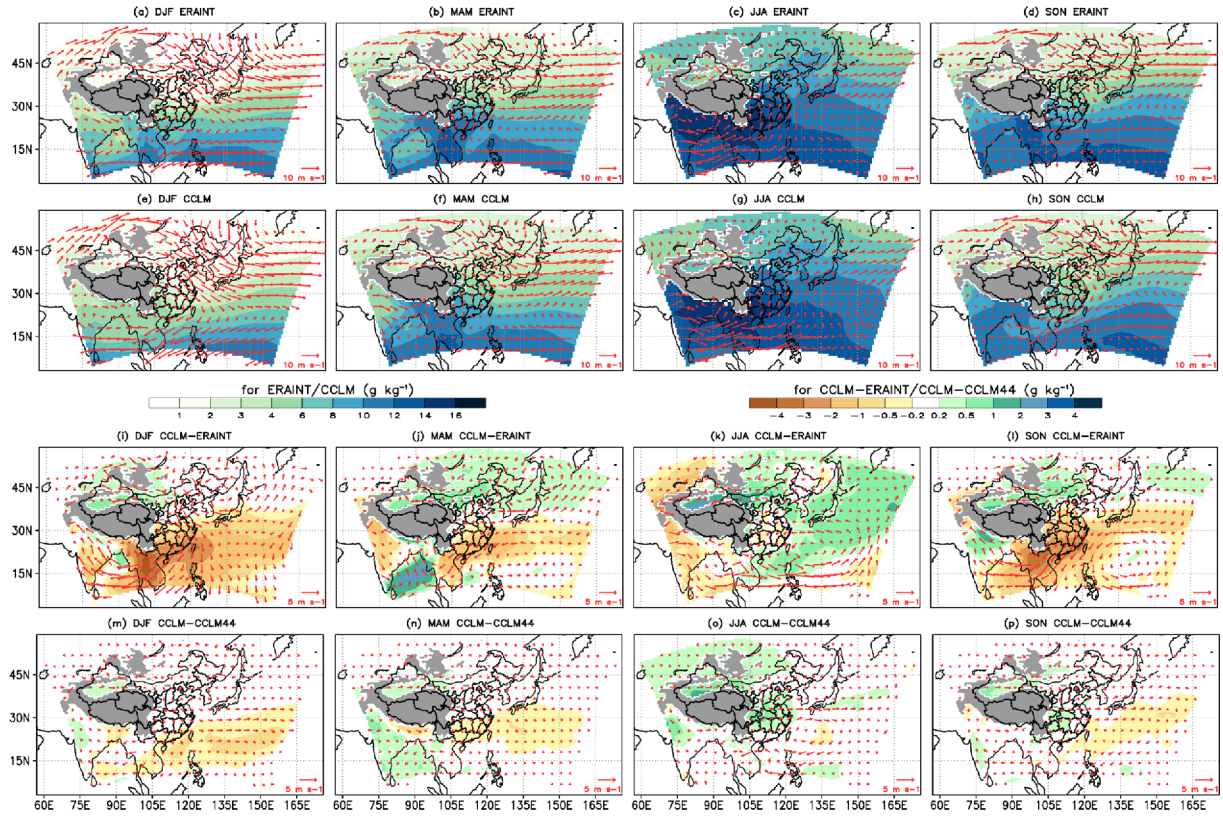

Fig. 11. Seasonal mean water vapor mixing ratio (shading, unit: g kg^{-1}) and vector winds (arrow, unit: m s^{-1}) at 850 hPa for the period 1989-2010. The rows are ERA-Interim reanalysis (ERAINT, top row), 0.22° CCLM simulations (CCLM, second row), CCLM bias against ERAINT (CCLM-ERAINT, third row), and 0.22° CCLM simulations difference against 0.44° CCLM simulations (CCLM-CCLM44, bottom row). The columns from left to right are for winter (DJF), spring (MAM), summer (JJA), and autumn (SON). The key vector wind is plotted at lower right corresponding to 10 m s^{-1} (ERAINT and CCLM) or 5 m s^{-1} (CCLM-ERAINT and CCLM-CCLM44). Grey zones indicate terrain height above 1600 m.

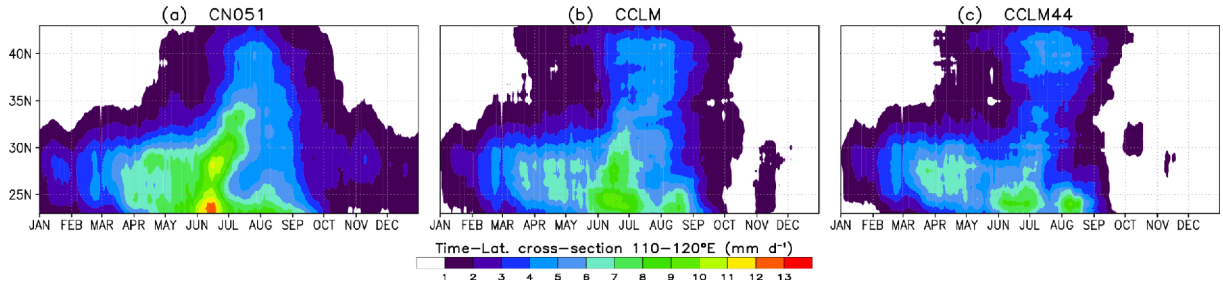

Fig. 12. Hovmoller diagrams of the mean annual precipitation cycle over eastern Mainland China (110-120°E average). A 20-d multi-year daily running mean has been used to remove high-frequency variability. The units are mm d^{-1}.

biases by the CCLM in intensity and frequency but negative biases for the duration (i.e., CWD and CDD), especially for CDD. In the aspect of domain-averaged values, the CCLM captures the interannual variation of the climate extreme indices fairly well with positive temporal correlations but tends to introduce warm and wet biases. This suggests that if future works, such as risk evaluation regarding climate extremes, are planned, bias correction techniques (e.g., Ahmed et al., 2013) could be important.

c. Large-scale circulation in the lower troposphere

To investigate the causes of the differences in the ability of the CCLM to simulate precipitation, the differences in the vector winds and the water vapor mixing ratio in the lower troposphere were analyzed between ERAINT reanalysis and CCLM simulations. Figure 11 shows the spatial distribution of the 22-year seasonal mean wind fields and mixing ratios at 850 hPa of ERAINT, CCLM, the differences between CCLM-ERAINT and CCLM-CCLM44.

In winter, the CCLM simulates a marked northerly wind bias (approximately 3-4 m s^{-1}) over South China and East China and an easterly wind bias (above 5 m s^{-1}) from the Indochina Peninsula to India. The overestimated anticyclonic circulation in the CCLM simulation could take more dry air from northern regions, resulting in a drier water vapor condition from India extending to the Pacific Ocean, which may partially contribute to the negative precipitation bias over these regions in winter. Similar CCLM bias patterns of underestimated-humidity-negative-precipitation-bias and overestimated-humidity-positive-precipitation-bias exist in most areas of the domain in all seasons, except in summer in the Northwestern Pacific, where the slightly underestimated humidity over the land and overestimated humidity over the sea by the CCLM are associated with a large area of negative precipitation bias. When the summer monsoon prevails and the quasi-stationary frontal system of the East Asian summer monsoon (EASM) is mostly disturbed by small transient cyclonic vortices (Wang, 2006), the leading cause of precipitation bias in this area could be the inadequate convective process in the CCLM suggested by Wang et al. (2013). In addition, the lowered mixing ratio and weakened southwesterly winds in the lower troposphere of the CCLM over South and East China land areas could still partially contribute to the underestimation of precipitation. The strong underestimation of precipitation in India in summer seems mainly due to the drier moisture bias simulated by the CCLM. In addition, the cyclonic wind bias over the Western Pacific Ocean may enhance the convective activity and thus increases the precipitation to the southwestern side of the Western Pacific Subtropical High (WPSH). In the autumn season (SON), this marked mean cyclonic wind bias in CCLM moves southeasterly with similar precipitation bias pattern around it.

While comparing the results of CCLM-CCLM44, the low-level cyclonic wind bias is obviously stronger in summer and autumn, CCLM44 (anticyclonic wind differences in Figs. 11o, p). It could be concluded that the higher resolution CCLM introduce some added values into the mean state of large scale circulation in the lower troposphere, at least for the rainy seasons.

d. East Asian summer monsoon

The East Asian climate is strongly influenced by the monsoon system (Wang, 2006), especially by the warm and wet EASM, which carries moist air from the Pacific Ocean and the Indian Ocean to East Asia, modulating the summer precipitation of Japan, Korea, the Philippines, Indochina, and most of China. Figure 12 shows the time-latitude Hovmoller diagram of the observed and simulated annual cycle of precipitation over eastern mainland China (110-120°E averaged). A 20-d daily running mean has been used to remove high-frequency variability. The result shows basic agreement between the CCLM simulations and the observations, especially in the time and latitude evolution of the monsoon precipitation.

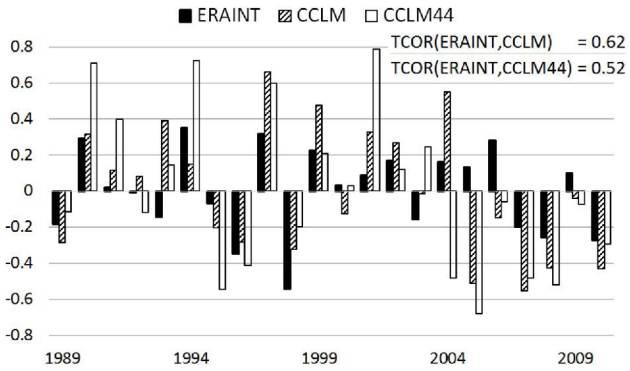

Fig. 13. Anomalies of the East Asian summer monsoon index for the period 1989-2010 (10°-40°N and 110°-140°E average, JJA mean; Li and Zeng, 2002) calculated from ERAINT and our RCM simulation (CCLM and CCLM44). The TCOR (correlation coefficient over time) is CCLM/CCLM44 against ERAINT.

However, a negative precipitation intensity bias by the CCLM exists in the south and a positive bias exists in the north. It is evident that the 0.22° CCLM exhibits better simulation performance for this monsoon-related annual precipitation cycle than the 0.44° CCLM44.

The interannual variability of the EASM is important to the precipitation in East Asia monsoon regions. For another simple assessment of the CCLM performance in the simulation of the EASM, an EASM index is used, which is derived from 850-hPa horizontal wind differences between the winter and summer seasons in the key area 10°-40°N, 110°-140°E (Li and Zeng, 2002). There are various types of EASM indices (Wang et al., 2008). The one we used in this study directly measures the strength of the low-level EASM winds using the 850-hPa southwesterly winds, thus a stronger-than-normal (positive anomaly) index is often associated with less precipitation over the mid-latitudes of East Asia, while other studies may define the strong/weak phases of the EASM in other ways (e.g., Lee et al., 2006; Cha et al. 2011). Figure 13 shows the time series of the EASM index anomaly from ERAINT and CCLM simulations. The CCLM is capable of capturing the main inter-annual variability feature of the EASM index with a temporal correlation above 0.6. The strong (e.g., 1990, 1997 and 1999) and weak (e.g., 1996, 1998, 2008 and 2010) EASM years are well reproduced. While this temporal correlation is lower between CCLM44 and ERAINT, it shows some added value from the higher resolution CCLM simulation in this study. However, it significantly overestimates the amplitude of the EASM variation, which could produce the large variance in precipitation (e.g., Fig. 5c).

The distribution of correlations between interannual EASM index and summer precipitation is presented in Fig. 14. The correlation coefficients between summer precipitation (GPCP) and EASM index (ERAINT) (Fig. 14a) clearly show the negative relationship in the middle and lower reaches of the Yangtze River in China and obvious positive relationship in the vicinity of the Philippines as well as the warm pool region

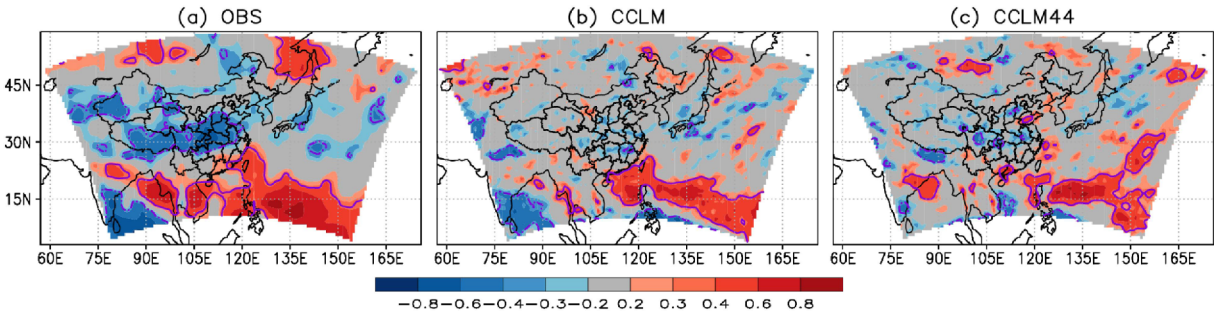

Fig. 14. Correlations between the EASM index (Li and Zeng, 2002) and the summer (JJA) precipitation for the period 1989-2010 over the CORDEX-EA-II domain. The EASM index of (a) OBS is calculated from ERAINT, the precipitation of OBS is from GPCP v2.2; the EASM index and precipitation of (b) CCLM and (c) CCLM44 are calculated from out RCM simulations. The dark colored areas inside the purple contours indicate the critical values of the correlation above the 90% confidence level.

in the Western Pacific Ocean, similar to previous studies (e.g., Li and Zeng, 2002). This remarkable positive correlation over the Philippines and the Western Pacific Ocean is reproduced by the CCLM, but the negative correlation over the middle and lower reaches of the Yangtze River is not that obvious. This result is consistent with the previous sections of this paper, e.g., the worse simulation of the interannual variability of the summer precipitation in East China (Fig. 5c). The CCLM still assembles correlation map patterns slightly better than the coarser CCLM44 simulation.

4. Summary, discussion and concluding remarks

In this paper, we present the CCLM regional climate simulation with the high resolution of 0.22° (~25 km) over the CORDEX-EA-II domain. The simulation is performed for the period 1988-2010 driven by the ERA-Interim reanalysis datasets. The CCLM model is thoroughly evaluated by analyzing the ability of the model to simulate mean states, annual cycles, interannual variations and climate extremes of both surface air temperature and precipitation, as well as the associated general circulations and East Asian summer monsoon index. Various observed datasets are employed for the validation, including gridded data interpolated from station observations, satellite-based products and reanalysis data. Some results from a parallel but coarser resolution simulation at 0.44° (~50 km) are also presented.

In general, the CCLM is able to capture the overall features of the seasonal temperature and precipitation. The bias of the simulated surface air temperature ranges from −3.0°C to +3.0°C, but it is notably warmer by 5.0°C in the northern arid and semi-arid areas of the CORDEX-EA-II domain and in India and colder by −5.0°C in the Himalayas region, especially in the winter season. Most of the wet biases appear in arid areas, the Tibetan Plateau and summer tropics, while dry biases occur over India and the oceans in winter. The bias patterns show some similarities to previous studies adopting CCLM in this area with different domain settings and driving datasets (e.g., Wang et al., 2013; Bucchignani et al., 2014; Huang et al., 2015).

The marked cold biases in the Tibetan and other high altitude areas may be partially inherited from the ERA-Interim data (Zou et al., 2014b), and partially due to the underestimation of the model orography (Bucchignani et al., 2014). Another possible key bias source could be the land surface interaction and parameterization scheme, some recent studies (e.g., Panitz et al., 2014; Bucchignani et al., 2015b) found that with modified parameterization of the soil albedo data, the CCLM model can reduces bias, particular the positive temperature biases over desert areas in Africa and the Middle East. Concerning precipitation, Wang et al. (2013) suggested that while the performance of the CCLM in the simulation of dominant monsoon circulations is fairly good, the negative precipitation bias over southeastern domain areas might result from the inadequate parameterization of the convection scheme for the precipitation processes or to the insufficient resolution of the tropopause height, which is constant in the CCLM model. The positive precipitation bias in the northern domain areas might come from the moisture not condensing to precipitation in the south. Wang et al. (2013) and Bucchignani et al. (2014) suggested the underestimation of orographic effects with coarser resolution grids might also partly contribute to the bias of precipitation. In our study, we also found that the CCLM shows low-level anticyclonic wind biases over land areas in winter and cyclonic bias over the Northwestern Pacific Ocean from spring to autumn and that less water vapor transports to East China and South China due to weaker southwesterly winds in summer, which could also contribute the underestimation of the precipitation there. Besides that, the relationship of evident wet and cold bias in high altitude areas and colder seasons (e.g., the Tibetan Plateau in winter) might be partially explained by the snow cover, moisture and evaporation feedbacks, as suggested by Haslinger et al. (2013) while analyzing the CCLM simulations over the Alps.

The CCLM is also able to reproduce the annual cycles and the interannual variabilities of the temperature and precipitation, although the results spread among regions. The simulated interannual variances are generally higher than observations, especially for the seasonal precipitation, which also agrees with other previous studies using the CCLM in this

area (e.g., Huang et al., 2015). The climate extreme indices derived from daily temperature and precipitation show good agreement between the simulation and the observation with high correlation coefficients. The CCLM tends to generate relatively hotter indices for temperature and wetter indices for precipitation compared with the results of the domain average.

Considering the fact that the interannual variation of the summer precipitation contributes most to this area, the CCLM simulation resembles the observed positive correlation between the EASM index and the precipitation over the Philippines and the Western Pacific Ocean fairly well, but the negative correlation over the middle and lower reaches of the Yangtze River is not reproduced significantly, suggesting that further investigations are needed in the future.

The comparison of the 0.44° and 0.22° simulations revealed some added value from the use of the higher resolution CCLM configuration in the CORDEX-EA-II domain, including less bias in the mean temperature and precipitation, especially in the center of the model domain and the summer season. In addition, the 0.22° simulation shows better performance than the 0.44° simulation for the prediction of the mean monsoon precipitation evolution over eastern Mainland China and a higher correlation between the interannual variation of the EASM index and the summer precipitation over the domain. These preliminary results suggest that the increase in computational time could be offset by the improvement in the performance of the higher resolution CORDEX-EA-II framework using the CCLM model.

Some general concluding remarks can be drawn for this work:

(1) The CCLM model can reproduce the major climate features fairly well in East Asia, including the mean and extreme climate status, and the new 0.22° high resolution shows some added value over the coarser 0.44° resolution. Thus, the CCLM could be an adequate member of the next phase of the CORDEX-EA initiative (i.e., an ensemble member of the multiple RCM comparisons and a dynamical downscaling tool for projecting future scenarios based on GCM outputs).

(2) There are some obvious biases in the CCLM regional climate simulation over East Asia in certain regions and seasons. Further studies are needed to investigate the areas with large biases, the roles of the parameterization schemes, and the possible added values by the RCMs.

Acknowledgements. This work is supported by the National Natural Science Foundation of China (41375075, 91425304, 41575099, and 91525101). The authors acknowledge with thanks the ECMWF, the COSMO-CLM community, and the German Climate Computing Center (DKRZ) for providing the processed ERA-Interim reanalysis data. The authors also appreciate the National Climate Center (CMA) for providing the gridded surface observation datasets over China. In addition, we declare that we have no conflict of interest.

Edited by: Song-You Hong, Kim and Yeh

References

AghaKouchak, A., D. Easterling, K. Hsu, S. Schubert, and S. Sorooshian, Eds., 2013: *Extremes in a changing climate: detection, analysis and uncertainty*. Water Science and Technology Library, Vol. 65, Springer Netherlands, 426 pp.

Ahmed, K. F., G. Wang, J. Silander, A. M. Wilson, J. M. Allen, R. Horton, and R. Anyah, 2013: Statistical downscaling and bias correction of climate model outputs for climate change impact assessment in the U.S. northeast. *Glob. Planet. Change*, **100**, 320-332.

Arakawa, A., and V. R. Lamb, 1977: Computational design of the basic dynamical processes of the UCLA general circulation model. *Methods in Computational Physics*, **17**, 173-265.

Bowden, J. H., T. L. Otte, C. G. Nolte, and M. J. Otte, 2012: Examining interior grid nudging techniques using two-way nesting in the WRF model for regional climate modeling. *J. Climate*, **25**, 2805-2823.

Bucchignani, E., M. Montesarchio, L. Cattaneo, M. P. Manzi, and P. Mercogliano, 2014: Regional climate modeling over China with COSMO-CLM: Performance assessment and climate projections. *J. Geophys. Res. Atmos.*, **119**, 12151-12170.

_____, _____, A. L. Zollo, and P. Mercogliano, 2015a: High-resolution climate simulations with COSMO-CLM over Italy: performance evaluation and climate projections for the 21st century. *Int. J. Climatol.*, **36**, 735-756.

_____, L. Cattaneo, H.-J. Panitz, and P. Mercogliano, 2015b: Sensitivity analysis with the regional climate model COSMO-CLM over the CORDEX-MENA domain. *Meteorol. Atmos. Phys.*, **128**, 73-95.

Bukovsky, M. S., and D. J. Karoly, 2009: Precipitation simulations using WRF as a nested regional climate model. *J. Appl. Meteor. Climatol.*, **48**, 2152-2159.

Castro, C. L., R. A. Pielke Sr., and G. Leoncini, 2005: Dynamical downscaling: Assessment of value retained and added using the Regional Atmospheric Modeling System (RAMS). *J. Geophys. Res.*, **110**, D05108, doi:10.1029/2004JD004721.

Cha, D.-H., C.-S. Jin, and D.-K. Lee, 2011: Impact of local SST anomaly over the western North Pacific on extreme East Asian summer monsoon. *Clim. Dynam*., **37**, 1691-1705.

Dee, D. P., and Coauthors, 2011: The ERA-Interim reanalysis: configuration and performance of the data assimilation system. *Quart. J. Roy. Meteor. Soc.*, **137**, 553-597.

Dickinson, R. E., R. M. Errico, F. Giorgi, and G. T. Bates, 1989: A regional climate model for the western United States. *Climatic Change,* **15**, 383-422.

Dobler, A., and B. Ahrens, 2010: Analysis of the Indian summer monsoon system in the regional climate model COSMO-CLM. *J. Geophys. Res.*, **115**, D16101, doi:10.1029/2009JD013497.

Doms, G., and Coauthors, 2011: *A description of the nonhydrostatic regional COSMO model part II: physical parameterization*. DWD, Offenbach, Germany, 161 pp. [Available online at http://www.cosmo-model.org/content/model/documentation/core/].

_____, and M. Baldauf, 2015: *A description of the nonhydrostatic regional COSMO model part I: dynamics and numerics*. DWD, Offenbach, Germany, 164 pp. [Available online at http://www.cosmo-model.org/content/model/documentation/core/].

Dosio, A., H. J. Panitz, M. Schubert-Frisius, and D. Lüthi, 2015: Dynamical downscaling of CMIP5 global circulation models over CORDEX-Africa with COSMO-CLM: evaluation over the present climate and analysis of the added value. *Clim. Dynam*., **44**, 2637-2661.

Frich, P., L. V. Alexander, P. Della-Marta, B. Gleason, M. Haylock, A. M. G. Klein Tank, and T. Peterson, 2002: Observed coherent changes in climatic extremes during the second half of the twentieth century. *Clim.*

Res., **19**, 193-212.

Fu, C., and Z. Zheng, 1998: Monsoon regions: The highest rate of precipitation changes observed from global data. *Chinese Sci. Bull.*, **43**, 662-666.

_____, S. Wang, Z. Xiong, W. J. Gutowski, D.-K. Lee, J. L. McGregor, Y. Sato, H. Kato, J.-W. Kim, and M.-S. Suh, 2005: Regional Climate Model Intercomparison Project for Asia. *Bull. Amer. Meteor. Soc.*, **86**, 257-266.

Gao, X., Y. Xu, Z. Zhao, J. S. Pal, and F. Giorgi, 2006: On the role of resolution and topography in the simulation of East Asia precipitation. *Theor. Appl. Climatol.*, **86**, 173-185.

Giorgi, F., and G. T. Bates, 1989: The climatological skill of a regional model over complex terrain. *Mon. Wea. Rev.*, **117**, 2325-2347.

_____, and L. O. Mearns, 1999: Introduction to special section: Regional climate modeling revisited. *J. Geophys. Res.*, **104**, 6335-6352.

_____, C. Jones, and G. Asrar, 2009: Addressing climate information needs at the regional level: the CORDEX framework. *WMO Bull.*, **58**, 175-183.

_____, and W. J. Gutowski, Jr., 2015: Regional Dynamical Downscaling and the CORDEX Initiative. *Annu. Rev. Environ. Resour.*, **40**, 467-490.

Harris, I., P. D. Jones, T. J. Osborn, and D. H. Lister, 2014: Updated high-resolution grids of monthly climatic observations - the CRU TS3.10 Dataset. *Int. J. Climatol.*, **34**, 623-642.

Haslinger, K., I. Anders, and M. Hofstätter, 2013: Regional climate modelling over complex terrain: an evaluation study of COSMO-CLM hindcast model runs for the Greater Alpine Region. *Clim. Dynam*., **40**, 511-529.

Hong, S.-Y., and E.-C. Chang, 2012: Spectral nudging sensitivity experiments in a regional climate model. *Asia-Pac. J. Atmos. Sci.*, **48**, 345-355.

_____, and M. Kanamitsu, 2014: Dynamical downscaling: Fundamental issues from an NWP point of view and recommendations. *Asia-Pac. J. Atmos. Sci.*, **50**, 83-104.

Huang, B., S. Polanski, and U. Cubasch, 2015: Assessment of precipitation climatology in an ensemble of CORDEX-East Asia regional climate simulations. *Clim. Res.*, **64**, 141-158.

Huffman, G. J, R. F. Adler, D. T. Bolvin, and G. Gu, 2009: Improving the Global Precipitation Record: GPCP Version 2.1. *Geophys. Res. Lett.*, **36**, L17808, doi:10.1029/2009GL040000.

Im, E.-S, B.-J. Lee, J.-H. Kwon, S.-R. In, and S.-O. Han, 2012a: Potential increase of flood hazards in Korea due to global warming from a high-resolution regional climate simulation. *Asia-Pac. J. Atmos. Sci.*, **48**, 107-113.

_____, J.-B. Ahn, and D.-W. Kim, 2012b: An assessment of future dryness over Korea based on the ECHAM5-RegCM3 model chain under A1B emission scenario. *Asia-Pac. J. Atmos. Sci.*, **48**, 325-337.

IPCC, 2013: *Climate Change 2013: The Physical Science Basis*. *Contribution of Working Group I to the Fifth Assessment Report of the Intergovernmental Panel on Climate Change*. Cambridge University Press, 1535 pp.

_____, 2014: *Climate Change 2014: Impacts, Adaptation, and Vulnerability. Part B: Regional Aspects. Contribution of Working Group II to the Fifth Assessment Report of the Intergovernmental Panel on Climate Change*. Cambridge University Press, 688 pp.

Jaeger, E. B., I. Anders, D. Lüthi, B. Rockel, C. Schär, and S. I. Seneviratne, 2008: Analysis of ERA40-driven CLM simulations for Europe. *Meteorol. Z.*, **17**, 349-367.

Jones, P. W., 1999: First- and second-order conservative remapping schemes for grids in spherical coordinates. *Mon. Wea. Rev.,* **127**, 2204-2210.

Kothe, S., D. Lüthi, and B. Ahrens, 2014: Analysis of the West African Monsoon system in the regional climate model COSMO-CLM. *Int. J. Climatol.*, **34**, 481-493.

Lee, E.-J., S.-W. Yeh, J.-G. Jhun, and B.-K. Moon, 2006: Seasonal change in anomalous WNPSH associated with the strong East Asian summer monsoon. *Geophys. Res. Lett.*, **33**, L21702, doi:10.1029/2006GL027474.

Lee, D.-K., D.-H. Cha, C.-S. Jin, and S.-J. Choi, 2013: A regional climate change simulation over East Asia. *Asia-Pac. J. Atmos. Sci.*, **49**, 655-664.

Lee, J.-W., S.-Y. Hong, E.-C. Chang, M.-S. Suh, and H.-S. Kang, 2014: Assessment of future climate change over East Asia due to the RCP scenarios downscaled by GRIMs-RMP. *Clim. Dyn.*, **42**, 733-747.

Li, J. P., and Q. C. Zeng, 2002: A unified monsoon index. *Geophys. Res. Lett.*, **29**, doi:10.1029/2001GL013874.

Mironov, D., and M. Raschendorfer, 2001: *Evaluation of empirical parameters of the new LM surface-layer parameterization Scheme: results from numerical experiments including soil moisture analysis*. COSMO technical report No.1. DWD, Offenbach, Germany, 12 pp. [Available online at http://www.cosmo-model.org/content/model/documentation/techReports/docs/techReport01.pdf].

Montesarchio, M., A. L. Zollo, E. Bucchignani, P. Mercogliano, and S. Castellari, 2014: Performance evaluation of high-resolution regional climate simulations in the Alpine space and analysis of extreme events. *J. Geophys. Res*., **119**, 3222-3237.

Oh, S.-G., J.-H. Park, S.-H. Lee, and M.-S. Suh, 2014: Assessment of the RegCM4 over East Asia and future precipitation change adapted to the RCP scenarios. *J. Geophys. Res*., **119**, 2913-2927.

Panitz, H. J., A. Dosio, M. Büchner, D. Lüthi, and K. Keuler, 2014: COSMO-CLM (CCLM) climate simulations over CORDEX-Africa domain: analysis of the ERA-Interim driven simulations at 0.44° and 0.22° resolution. *Clim. Dyn.*, **42**, 3015-3038.

Park, J.-H., S.-G. Oh, and M.-S. Suh, 2013: Impacts of boundary conditions on the precipitation simulation of RegCM4 in the CORDEX East Asia domain. *J. Geophys. Res*., **118**, 1652-1667.

Ritter, B., and J. F. Geleyn, 1992: A comprehensive radiation scheme for numerical weather prediction models with potential applications in climate simulations. *Mon. Wea. Rev.*, **120**, 303-325.

Rockel, B., A. Will, and A. Hense, 2008: The regional climate model COSMO-CLM (CCLM). *Meteorol. Z.*, **17**, 347-348.

_____, and B. Geyer, 2008: The performance of the regional climate model CLM in different climate regions, based on the example of precipitation. *Meteorol. Z.*, **17**, 487-498.

Rummukainen, M., 2010: State-of-the-art with regional climate models. *WIREs Clim. Change*, **1**, 82-96.

Schrodin, R., and E. Heise, 2001: *The Multi-Layer Version of the DWD Soil Model TERRA-LM*. COSMO Technical Report No. 2, DWD, offenhach, Germany, 16 pp. [Available online at http://www.cosmo-model.org/content/model/documentation/techReports/docs/techReport02.pdf].

Seifert, A., and K. D. Beheng, 2001: A double-moment parameterization for simulating autoconversion, accretion and selfcollection. *Atmos. Res.*, **59-60**, 265-281.

Sillmann, J., V. V. Kharin, F. W. Zwiers, X. Zhang, and D. Bronaugh, 2013: Climate extremes indices in the CMIP5 multimodel ensemble: Part 2. Future climate projections. *J. Geophys. Res*., **118**, 2473-2493.

Smiatek, G., 2014: Time invariant boundary data of regional climate models COSMO-CLM and WRF and their application in COSMO-CLM. *J. Geophys. Res*., **119**, 7332-7347.

Suh, M.-S., and D.-K. Lee, 2004: Impacts of land use/cover changes on surface climate over east Asia for extreme climate cases using RegCM2. *J. Geophys. Res.*, **109**, D02108, doi:10.1029/2003JD003681.

Sun, Q. H., C. Y. Miao, Q. Y. Duan, D. X. Kong, A. Z. Ye, Z. H. Di, and W. Gong, 2014: Would the 'Real' Observed Dataset Stand Up? A Critical Examination of Eight Observed Gridded Climate Datasets for China. *Environ. Res. Lett.*, **9**, 015001, doi:10.1088/1748-9326/9/1/015001.

Taylor, K. E., 2001: Summarizing multiple aspects of model performance

in a single diagram. *J. Geophys. Res.*, **106**, 7183-7192.

Tiedtke, M., 1989: A comprehensive mass flux scheme for cumulus parameterization in large-scale models. *Mon. Wea. Rev.*, **117**, 1779-1800, doi:10.1175/1520-0493(1989)117<1779:ACMFSF>2.0.CO;2.

Wang, B., Ed., 2006: *The Asian Monsoon*. Springer/Praxis Publishing Co., New York, pp. 788, doi:10.1007/3-540-37722-0.

_____, Z. Wu, J. Li, J. Liu, C.-P. Chang, Y. Ding, and G. Wu, 2008: How to measure the strength of the East Asian summer monsoon. *J. Climate*, **21**, 4449-4463.

Wang D., C. Menz, T. Simon, C. Simmer, and C. Ohlwein, 2013: Regional dynamical downscaling with CCLM over East Asia. *Meteorol. Atmos. Phys.*, **121**, 39-53.

Wicker, L. J., and W. C. Skamarock, 2002: Time-splitting methods for elastic models using forward time schemes. *Mon. Wea. Rev.*, **130**, 2088-2097.

Wu, J., and X. J. Gao, 2013: A gridded daily observation dataset over China region and comparison with the other datasets. *Chinese J. Geophys*., **56**, 1102-1111 (in Chinese).

Xue, Y., Z. Jajnic, J. Dudhia, R. Vasic, and F. De Sales, 2014: A review on regional dynamical downscaling in intra-seasonal to seasonal simulation/prediction and major factors that affect downscaling ability. *Atmos. Res.*, **147-148**, 68-85.

Yun, K.-S., K.-Y. Heo, J.-E. Chu, K.-J. Ha, E.-J. Lee, Y. Choi, and A. Kitoh, 2012: Changes in climate classification and extreme climate indices from a high-resolution future projection in Korea. *Asia-Pac. J. Atmos. Sci.*, **48**, 213-226.

Zhao, D., 2013: Performance of Regional Integrated Environment Modeling System (RIEMS) in precipitation simulations over East Asia. *Clim. Dyn.*, **40**, 1767-1787.

Zou, L., Y. Qian, T. Zhou, and B. Yang, 2014a: Parameter Tuning and Calibration of RegCM3 with MIT-Emanuel Cumulus Parameterization Scheme over CORDEX East Asia Domain. *J. Climate*, **27**, 7687-7701.

Zou, H., J. Zhu, L. Zhou, P. Li, and S. Ma, 2014b: Validation and application of reanalysis temperature data over the Tibetan plateau. *J. Meteorol. Res.*, **28**, 139-149.